

Electronic Thesis and Dissertation Repository

12-15-2016 12:00 AM

Investigation of Grouted Dowel Connection for Precast Concrete Wall Construction

Douglas J. Provost-Smith, *The University of Western Ontario*

Supervisor: Dr. Moncef Nehdi, *The University of Western Ontario*

A thesis submitted in partial fulfillment of the requirements for the Master of Engineering Science degree in Civil and Environmental Engineering

© Douglas J. Provost-Smith 2016

Follow this and additional works at: <https://ir.lib.uwo.ca/etd>



Part of the [Civil Engineering Commons](#), [Construction Engineering and Management Commons](#), and the [Structural Engineering Commons](#)

Recommended Citation

Provost-Smith, Douglas J., "Investigation of Grouted Dowel Connection for Precast Concrete Wall Construction" (2016). *Electronic Thesis and Dissertation Repository*. 4298.
<https://ir.lib.uwo.ca/etd/4298>

This Dissertation/Thesis is brought to you for free and open access by Scholarship@Western. It has been accepted for inclusion in Electronic Thesis and Dissertation Repository by an authorized administrator of Scholarship@Western. For more information, please contact wlsadmin@uwo.ca.

ABSTRACT

The grouted dowel connection is a simple and cost-effective connection used in many precast concrete structural systems. The required dowel length is currently designed as a regular bar in reinforced concrete, which underestimates the bond strength, thus resulting in excessive connection lengths. Furthermore, precast wall construction continues throughout cold weather, where in-situ heating of the grout used in the grouted dowel connections is usually conducted for short periods of time. Hence, early-age exposure to subfreezing conditions may affect the quality of the grout and subsequently the bond strength of the connection, which can compromise structural integrity.

In this thesis, representative pullout tests were performed and their results were compared with relevant data in the open literature in order to develop a reliable design equation for predicting the required dowel development length. The equation was found to produce results three times smaller than that determined by the ACI 318-14 code, while being desirably 10% more conservative than equations proposed in previous research.

The effect of subfreezing exposure on the bond strength of the connection, along with the mechanical properties, hydration process and pore size distribution of the grout were also examined. Grout specimens were initially cured at ambient temperature ($23 \pm 1^\circ\text{C}$) for one day and then placed inside an environmental chamber at -10°C . The compressive strength of the grout was monitored at additional temperatures of 1°C and -20°C . It was found that early-age subfreezing curing temperatures reduced the compressive strength of the grout, leading to increased dowel embedment length to achieve bar fracture. The bond strength of the connection remained proportional to the square root of compressive strength, even when subsequent to early-age subfreezing exposure.

Keywords: Precast concrete, bond strength, connection, grout, duct, development length, cold weather, curing, compressive strength, low temperature.

CO-AUTHORSHIP STATEMENT

All experimental work, data analysis, and writing of the initial versions of this thesis were performed by Douglas Provost-Smith. Mohamed Elsayed helped in conducting the pullout tests. Dr. Moncef Nehdi developed the original concept of the project and created the relationship with, and ensured the support from, the Industry Partner of this project, who fabricated full-scale test specimens at their Precast Plant. He also provided guidance and supervision, and helped in the development of the final versions of the publications.

Chapter 3 of this thesis was submitted for peer review and possible publication in the *ACI Structural Journal*. Chapter 4 of this thesis was submitted for peer review and possible publication to the *Construction and Building Materials Journal*. An abridged version of Chapter 4 of this thesis was published as part of the 5th International Materials Specialty Conference of the Canadian Society for Civil Engineering in London, Ontario, June 2016.

ACKNOWLEDGMENTS

I would like to express my sincerest thanks to my supervisor Dr. Moncef L. Nehdi. His guidance, advice, and encouragement have been incredibly valuable and instrumental to the completion of my thesis.

Thank you to Mohamed (Gamal) Elsayed for his continued support. He provided valuable discussions, and helped with experiments in the Structures Laboratory.

I would like to thank Wilber Logan for his assistance, suggestions, and valuable insight throughout my experimental work.

I am grateful to Stubbe's Precast for their strong support of this project. Manufacturing the test specimens at their precast plant in Harley, Ontario was crucial for the progress of these experiments.

Thank you to all the staff in the Department of Civil and Environmental Engineering for the continued support throughout my period of study.

Finally, I would like to thank my Grandparents, who have always been my biggest supporters. I would not be where I am today without you.

TABLE OF CONTENTS

Abstract	ii
Co-Authorship Statement.....	iii
Acknowledgments.....	iv
Table of Contents	v
List of Tables	viii
List of Figures	x
Nomenclature	xii
1 Introduction	1
1.1 Background.....	1
1.2 Cold Weather Construction.....	3
1.3 Research Objectives.....	4
1.4 Outline of Thesis.....	4
1.5 References.....	5
2 Literature Review	6
2.1 Introduction.....	6
2.2 Bond.....	7
2.2.1 Confinement.....	8
2.3 Precast Wall Connections	10
2.3.1 Post-Tensioning	10
2.3.2 Grouted Splice Sleeves	11
2.3.3 Grouted Dowels	12
2.4 Cold Weather Curing of Concrete	15
2.4.1 Effect on Compressive Strength	15

2.4.2	Effect on Bond Strength.....	19
2.5	References.....	20
3	Investigation of Grouted Dowel Connections for Precast Concrete Wall Panels.....	23
3.1	Introduction.....	23
3.2	Research Significance.....	26
3.3	Experimental Program	26
3.3.1	Test Specimens and Setup	26
3.4	Experimental Results and Discussion.....	28
3.4.1	Failure Modes	29
3.4.2	Effect of Duct.....	31
3.4.3	Effect of Eccentricity	34
3.4.4	Bond Behaviour	35
3.4.5	Analysis of Experimental Results.....	40
3.5	Comparisons with Current Design Equations.....	41
3.6	Future Research	43
3.7	Summary and Conclusions	43
3.8	References.....	44
4	Early-age Exposure of Grouted Precast Concrete Wall Connections to Subfreezing Curing Temperatures.....	46
4.1	Introduction.....	46
4.2	Research Significance.....	47
4.3	Experimental Investigation	48
4.4	Experimental Results and Discussion.....	51
4.4.1	Compressive Strength.....	51
4.4.2	Tensile Strength	55
4.4.3	Modulus of Elasticity	56

4.4.4	Thermogravimetric Analysis	57
4.4.5	Mercury Intrusion Porosimetry	59
4.4.6	Bond Behaviour of Grouted Dowel	61
4.5	Summary and Conclusions	67
4.6	References	68
5	Summary and Conclusions	72
5.1	Summary	72
5.2	Conclusions	74
5.3	Recommendations for Future Work	76
5.4	References	76
	Appendices	78
	Curriculum Vitae	92

LIST OF TABLES

Table 3.1: Pullout test results.....	29
Table 3.2: Normalized strength data.....	36
Table 4.1: Compressive strength of grout at various curing temperatures	52
Table 4.2: Grout tensile strength, Young’s modulus, and Poisson’s ratio.....	56
Table 4.3: Relative mass change (in %) and calculated content (in %) of the corresponding hydration products.....	59
Table 4.4: Average pore size and total intrusion volume from MIP test.....	60
Table 4.5: Pullout test results.....	61
Table A.1: Compressive strength data of concrete cured at ambient ($23 \pm 1^\circ\text{C}$)	78
Table A.2: Compressive strength data of concrete cured at 1°C	78
Table A.3: Compressive strength data of concrete cured at -10°C	79
Table A.4: Compressive strength data of concrete cured at -20°C	80
Table A.5: Tensile strength data of concrete cured at ambient ($23 \pm 1^\circ\text{C}$)	81
Table A.6: Tensile strength data of concrete cured at -10°C	81
Table A.7: Young’s Modulus data for ambient ($23 \pm 1^\circ\text{C}$) curing.....	82
Table A.8: Young’s Modulus data for -10°C curing	83
Table A.9: MIP data for grout cured for 1 day at ambient (23°C)	84
Table A.10: MIP data for grout cured for 7 days at ambient (23°C).....	86

Table A.11: MIP data for grout cured for 3 days at -10°C 88

Table A.12: MIP data for grout cured for 7 days at -10°C 90

LIST OF FIGURES

Figure 1.1: Typical grouted dowel connection.	2
Figure 2.1: Emulative precast wall connections using: a) grouted splice sleeve, and b) grouted dowels; c) Section A-A.....	7
Figure 2.2: Load transfer between deformed steel and concrete (ACI Committee 408, 2003).	8
Figure 3.1: Typical grouted dowel connection.	Error! Bookmark not defined.
Figure 3.2: Pullout test specimen and setup.....	27
Figure 3.3: Specimen damage: (a) hairline cracking of concrete block; (b) grout conical failure.	30
Figure 3.4: Splitting expansion failure of corrugated duct.	31
Figure 3.5: Tensile splitting failure of the concrete block for specimen 12CN-1.	32
Figure 3.6: Reduction in strength due to absence of duct and/or eccentricity.....	33
Figure 3.7: Tensile splitting through grout cylinder of specimen 12CN-1.....	33
Figure 3.8: Tensile splitting of surrounding concrete for specimen 12ED-1.	34
Figure 3.9: Tensile splitting through grout and surrounding concrete (specimen 12EN-2).	35
Figure 3.10: Bar stress-displacement plots for each embedment length.	37
Figure 3.11: Normalized bond stress-slip response for each embedment length.	38
Figure 3.12: Comparisons of current bond-slip models.....	39
Figure 3.13: Normalized bar stress versus normalized embedment length.	41

Figure 3.14: Predicted versus experimental peak bar stress comparison.....	42
Figure 4.1: Pullout test specimen and setup.....	51
Figure 4.2: Compressive strength development for various temperatures.	53
Figure 4.3: Internal grout temperature for varying subfreezing conditions.....	53
Figure 4.4: Ratio of compressive strength for varying initial curing periods to the 7-day strength of specimens initially cured for 1 day.	55
Figure 4.5: Ratio of 28-day to the 1-day tensile and compressive strengths for varying curing temperatures.....	56
Figure 4.6: DTG curves for grout specimens at different ages and curing conditions.	58
Figure 4.7: TGA curves for grout specimens at different ages and curing conditions.	58
Figure 4.8: Incremental pore intrusion volume versus pore diameter for grout specimens at different ages and curing conditions.	60
Figure 4.9: Bar stress-displacement plots for each embedment length and curing regime.	62
Figure 4.10: Failure modes of pullout specimens: (a) bar pullout; (b) bar fracture.....	63
Figure 4.11: Normalized bond stress versus normalized embedment length.	64
Figure 4.12: Bond stress-slip response for each embedment length and curing regime compared to established models.	66

NOMENCLATURE

d_b	= bar diameter
d_{duct}	= duct diameter
f_g'	= grout compressive strength
f_n	= confining pressure
f_s	= axial bar stress
f_y	= bar yield stress
l_d	= development length
l_{eff}	= effective length
l_{emb}	= embedment length
l_d/d_b	= normalized embedment length
P	= axial force at failure
R_s	= strength ratio
s	= bar slip
s_{max}	= bar slip at failure
u_b	= average bond stress at failure
$u_b/\sqrt{f_g'}$	= normalized bond stress
u_{eff}	= calculated effective bond stress at failure
$u_{eff}/\sqrt{f_g'}$	= normalized effective bond stress
α	= grout cone angle
δ_y	= yielding displacement

δ_u = ultimate displacement

μ_Δ = ductility ratio

1 INTRODUCTION

1.1 Background

Precast-concrete load-bearing wall panels have become a popular choice for low-, medium-, and high-rise construction in North America. The repetitive nature of this structural system allows for the mass production of high quality precast elements ready to be quickly assembled on site. These panels are precast in an environmentally controlled manufacturing facility, allowing for high quality control and constant production, regardless of weather conditions. They also offer ease and speed of erection on site; indeed, typical construction speeds of one floor per week and better are often achieved. The reduction in site formwork and site labour, along with the speed of construction, greatly reduce costs, often making it a more cost-effective alternative to traditional cast-in-place construction.

An integral part of this structural system, which needs particular attention, is the connections between individual panel units, since it directly affects the strength and stability of the structure. The horizontal connection of precast concrete load-bearing wall panels requires vertical continuity across joints. To achieve this, designers prefer to use emulative connections rather than jointed connections as they perform similarly to a cast-in-place structure, and can therefore be designed similarly. There are two common methods of achieving emulative wall panel connections: mechanical splices, also referred to as grouted splices; and the grouted dowel connection. There is much research demonstrating the feasibility of grouted splices (Einea, Yamane, & Tadros, 1995; Jansson, 2008; Ling, Ahmad, & Ibrahim, 2014). However, they generally have poor construction tolerances and are costly due to the laborious fabrication required.

In the grouted dowel connection, a reinforcing bar protruding from the lower wall panel is grouted into a corrugated steel duct cast into the upper wall panel, as shown in **Fig. 1.1**. This connection is advantageous owing to its simplicity, favourable construction tolerances, and cost-effectiveness. In this system, the grouted dowel carries the tensile forces across the wall panel connection. Since ductility is required in this system, dowels

are required to undergo yielding, similar to regular reinforced concrete. Although there are specific code requirements for the use of mechanical splices, there are none for the use of the grouted dowel connection, and research on this connection is sparse.

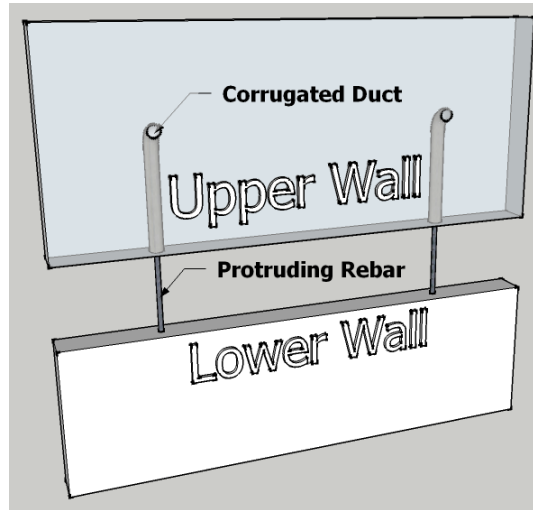


Figure 1.1: Typical grouted dowel connection.

Currently, this connection is designed using the development length equations for a regular reinforcing bar in concrete (ACI Committee 318, 2014). However, this design approach does not account for the additional confinement effect due to the presence of the corrugated steel duct. Research has shown that when greater confinement is provided, this method can lead to greatly oversized embedment lengths (Einea, Yehia, & Tadros, 1999).

Previous research on the use of this connection for precast bridge bent caps demonstrated that the ACI 318-05 Equation 12-1 produced development lengths three times longer than necessary (Steuck, Eberhard, & Stanton, 2009). However, the latter research was performed using larger diameter bars (32 mm to 57 mm) with larger duct diameter/bar diameter ratios of 3.6, whereas a typical wall panel connection uses a 25 mm diameter bar with a duct diameter/bar diameter ratio of 3.0. Steuck et al. (2009) research was also conducted with 55 MPa grout, and may not be accurate for lower grout strengths.

1.2 Cold Weather Construction

Another major advantage of the precast wall structural system is that construction can continue throughout adverse weather conditions, including cold weather. This is a particular advantage since Canada has a cold climate that experiences subfreezing temperatures over long periods of time, which can significantly slow or halt concrete construction. Winter construction of cast-in-place concrete requires the heating of large areas for extended periods of time, and typically involves the use of accelerators and/or other admixtures to ensure the development of adequate compressive strength. However, these methods can significantly increase energy consumption and cost, as well as make it difficult to maintain consistent quality control.

Although the construction of precast concrete wall panels can continue throughout cold weather conditions, the grouted dowel connection requires the placement of fresh grout. For this purpose, the entire floor is blanketed and heated while the grout is mixed and poured. After approximately one day, the heating is stopped and the connection is exposed to subfreezing temperatures before the grout is fully cured. This can significantly affect the quality of the grout and subsequently the bond strength of the connection, which can therefore compromise structural integrity.

Research on the effects of cold weather curing on the bond strength is sparse. The author could not access any studies in the open literature examining the effect of subfreezing curing on the bond strength. Rather, several researchers focus on the effects which subfreezing exposure had on the compressive strength of concrete since the latter is used to calculate the development length required based on the ACI 318-14 equation (25.4.2.3). However, Gardner and Poon (1976) investigated the effect of 2°C curing on the bond strength of concrete and concluded that the bond strength remained proportional to the square root of compressive strength, irrespective of the temperature or cement type. Yet, there is a need to further investigate this effect, especially for the grouted precast wall panel connection, where little is currently known.

1.3 Research Objectives

The primary objective of the research presented in this thesis is to acquire an advanced understanding of the behaviour of grouted dowel connections used in precast concrete wall panel construction. The specific research objectives are:

1. Conduct a thorough literature review to elucidate the mechanics of the grout-to-dowel bond, specifically in regards to confinement and failure modes.
2. Perform an experimental investigation on the grouted dowel connection specific to the precast wall panel connection, including the effects of early-age subfreezing exposure.
3. Analyze and compare experimental dowel pullout results to findings in existing literature to develop a design equation able to predict the required dowel development length for such a connection.
4. Quantify the effects of early-age exposure to subfreezing temperature on the bond strength of the connection, and provide recommendations for cold weather construction.

1.4 Outline of Thesis

This thesis is based on the “Integrated-Article Format” described in the Thesis Regulation Guide of Western University’s School of Graduate and Postdoctoral Studies. It includes five chapters that focus on the bond behaviour of the grouted dowel connection for use in precast concrete wall panels, and the effects of subfreezing exposure at early-age.

Chapter 2 provides a critical review of the mechanisms of bond, existing precast concrete wall panel connections, and the effect of cold weather curing on compressive strength and bond. Previous relevant investigations have been reviewed and discussed; with particular on the effects of variable cold weather curing on the compressive strength of concrete.

Chapter 3 examines the behaviour of the grouted dowel connection for use in precast wall panels. The results are analyzed and compared to existing data to develop a rational

design equation for predicting the required development length of this connection. A bond stress-slip model is also proposed and analysed in light of existing research.

Chapter 4 investigates the effects of exposure to early-age subfreezing temperature on the mechanical properties of the grout and the bond strength of the connection. The effect of subfreezing exposure is also examined on the development of hydration products and pore size distribution of the grout. The compressive strength of the grout was further investigated at varying curing regimes.

Chapter 5 presents a summary and the main conclusions drawn from the research study, along with recommendations for future research.

1.5 References

- ACI Committee 318. (2014). Building Code Requirements for Structural Concrete (ACI 318-14) and Commentary (ACI 318R-14). *American Concrete Institute*. Farmington Hills, MI.
- Einea, A., Yamane, T., & Tadros, M. K. (1995). Grout-filled pipe splices for precast concrete construction. *PCI Journal*, 40(1), 82–93.
- Einea, A., Yehia, S., & Tadros, M. K. (1999). Lap splices in confined concrete. *ACI Structural Journal*, 96(6), 947–955.
- Gardner, N. J., & Poon, S. M. (1976). Time and Temperature Effects on Tensile , Bond , and Compressive Strengths. *ACI Journal Proceedings*, 73(7), 405–409.
- Jansson, P. (2008). Evaluation of Grout-Filled Mechanical Splices for Precast Concrete Construction. *Michigan Department of Transportation*. Lansing, Michigan.
- Ling, J. H., Ahmad, A. B., & Ibrahim, I. S. (2014). Feasibility study of grouted splice connector under tensile load. *Construction and Building Materials*, 50, 530–539.
- Steuck, K. P., Eberhard, M. O., & Stanton, J. F. (2009). Anchorage of large-diameter reinforcing bars in ducts. *ACI Structural Journal*, 106(4), 506–513.

2 LITERATURE REVIEW

2.1 Introduction

Research on precast concrete wall connections began in the late 1980s when the benefits of precast concrete construction were beginning to be realized; the most prominent being the precast seismic structural system (PRESSS) research program. It spanned over 10 years and concluded with the testing of a five-story precast building constructed to 60 percent scale and tested using pseudo-dynamic loading. The building consisted of four different structural frame systems in one direction and a jointed structural wall system in the orthogonal direction. It was found that the building performed very well in both directions, with minimal damage to the shear wall despite seismic intensities reaching 50 percent above the design level (Priestley, Sritharan, Conley, & Pampanin, 1999). This research demonstrated the ability of precast concrete structural systems to be used instead of cast-in-place concrete, even under high levels of seismic excitation.

There are two types of precast concrete connections: jointed and emulative. Jointed connections usually consist of bolted or welded steel plates, where the connection stiffness differs from the wall stiffness, and therefore behaves differently from cast-in-place joints. The use of these types of connections requires experimental evidence under extreme loading conditions for special code acceptance. The research and labour required to install these connections can make them very costly. Hence, most designers tend to avoid them. Emulative connections are typically wet connections with rebar splicing. The ACI/ASCE Joint Committee 550 on Precast Concrete Structures defines emulative detailing as “the design of connection systems in a precast concrete structure so that its structural performance is equivalent to that of a conventionally designed cast-in-place, monolithic concrete structure” (ACI Committee 550, 2009). Since these connections perform comparably to cast-in-place connections, they may be designed in a similar manner; thus making such connections appealing to designers.

Typical emulative horizontal precast concrete wall connections consist of dry pack grout and vertical continuity reinforcement. Although there are many different variations to achieve continuity across the joint, three methods are commonly used: post-tensioning,

grouted splices sleeves (**Fig. 2.1a**), and grouted dowels (**Fig. 2.1b**). The first two will be briefly reviewed, while the third is the focus of the present research. These connections depend significantly on their bond, which is greatly increased by their high level of confinement. Therefore, to fully understand these connections, a review of bond from current research and relevant codes is first presented.

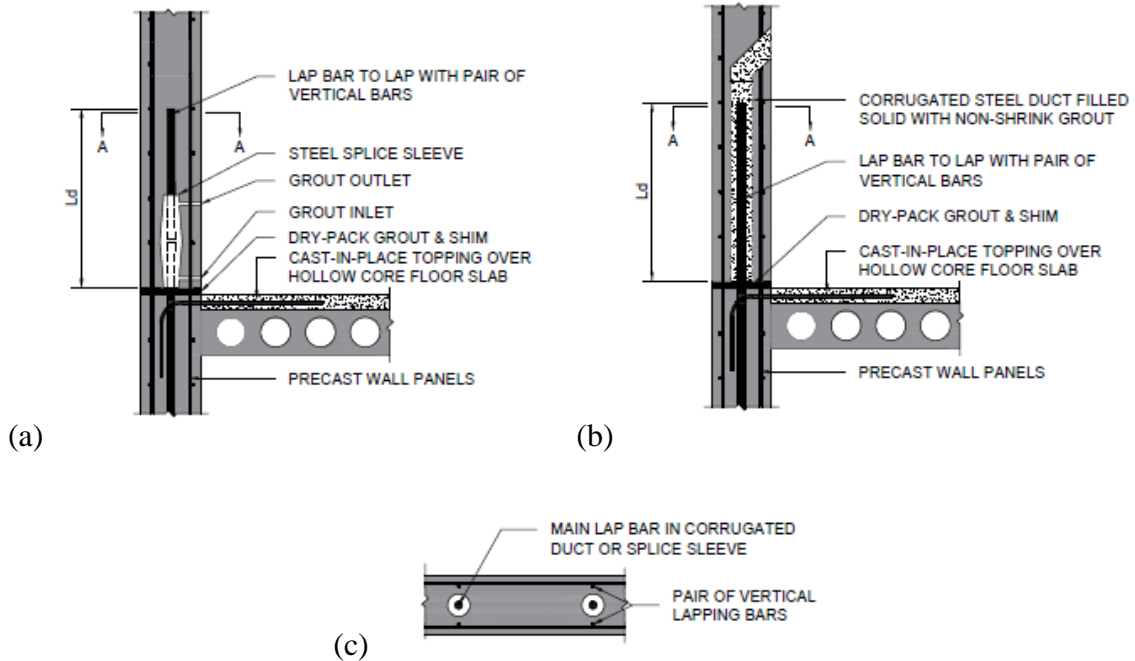


Figure 2.1: Emulative precast wall connections using: a) grouted splice sleeve, and b) grouted dowels; c) Section A-A.

2.2 Bond

The development length (l_d) – the length required to achieve bar yield – depends on the bond achieved between the bar and concrete, as well as the strength of the bar. Considering the bond of deformed steel bars in concrete, the load is transferred from the steel to the concrete through three mechanisms: chemical adhesion between the bar and the concrete; frictional forces between surface roughness of the bar and the concrete; and mechanical bearing of the deformed ribs against the concrete. This load transfer mechanism is illustrated in **Figure 2.2**. Once initial slip occurs, the chemical adhesion is lost and the load is transferred through friction and mechanical bearing. Furthermore,

since steel bars do not have significant roughness, mechanical bearing is the primary mode for load transfer. According to ACI Committee 408R-03, “the forces on the bar are balanced by compressive and shear stresses on the concrete contact surfaces, which are resolved into tensile stresses that can result in cracking planes that are perpendicular and parallel to the reinforcement” (ACI Committee 408, 2003).

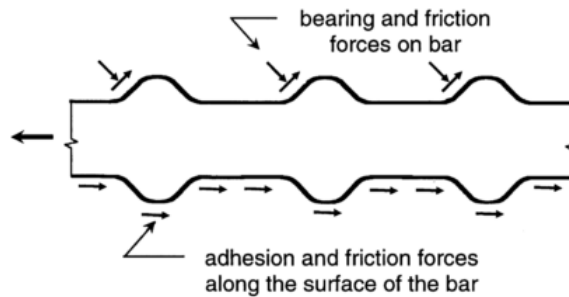


Figure 2.2: Load transfer between deformed steel and concrete (ACI Committee 408, 2003).

Bond failure can occur through tensile splitting of the concrete, or a pullout failure which results in shearing around the top surface of the ribs. The bond strength therefore depends on the strength and volume of the concrete surrounding the bar (which resists the tensile stresses), the surface deformations of the steel (which determine the concrete bearing area), and the degree of confinement (which help prevent tensile splitting). Although the two separate failure modes are known, bond failure can result from a combination of both modes, making the bond behaviour of reinforcing bars in concrete very complex. This is indicative of: the lack of mechanical design approach available for development lengths, with the current models based on statistical regression analyses (ACI Committee 318, 2014; Orangun, Jirsa, & Breen, 1977), and the constant changes regarding development lengths being made to ACI 318. Therefore, to accurately understand the bond behaviour of specific connection details, representative testing must be done.

2.2.1 Confinement

The most common methods to increase confinement of reinforcement bonded in concrete are through the use of transverse reinforcement (Soroushian, Choi, Park, & Aslani, 1991),

steel spirals (Hosseini, Rahman, Osman, Saim, & Adnan, 2015), steel pipes (Einea et al., 1995), or increased concrete cover. These methods are provide passive confinement, since they are reactionary in nature, and contribute through controlling propagation of splitting cracks. Passive confinement allows the bar to fail in a shearing pullout failure instead, which occurs at higher loads. When steel pipes have been used, their reactionary confinement stresses have led to higher frictional resistance of the bar, resulting in much shorter development lengths than in traditional reinforced concrete (Einea et al., 1995).

Active confinement is a method of applying normal pressure to the bonded reinforcing bar. Untrauer and Henry (1965) tested 37 pull-out specimens with varying degrees of normal pressure (0 to $0.5f'_c$) applied to two parallel faces of the bond specimen. More recently, Moosavi et al. (2005) improved on this test by applying a uniform radial confinement pressure to grouted rock bolt bond specimens. In both studies the confinement pressure was shown to increase the bond strength by increasing the bars frictional resistance and controlling tensile splitting of the concrete. Although it is difficult to actively confine reinforcement, the principles discovered here can be used to analyze reactionary confinement stresses generated through different passive confinement techniques. Untrauer and Henry (1965) developed an equation (**Eq. 2.1**) to predict the ultimate bond capacity, u_b , based on the confining pressure and the concrete compressive strength. This equation is the basis for determining the confinement effects of many new precast grouted connections.

$$u_b = (18.0 + 0.45\sqrt{f_n})\sqrt{f'_c} \quad (2.1)$$

Where,

u_b = ultimate bond strength (psi);

f_n = confining pressure (psi);

f'_c = concrete compressive strength (psi).

2.3 Precast Wall Connections

A review of the three most common emulative precast wall connections is presented with a focus on the grouted dowel connection. To make comparisons between different bar sizes easier, researchers normalize the embedment length in terms of the bar diameter (d_b), and will be discussed similarly herein.

2.3.1 Post-Tensioning

The applicability of bonded post-tensioned shear walls has been previously demonstrated (Hutchinson, Rizkalla, Lau, & Heuvel, 1991); nine different specimens were tested under monotonic shear loading and equations to accurately predict their shear capacity were developed. This research was continued by testing three different post-tensioning configurations: bonded post-tensioned strands, bonded post-tensioned bars, and unbonded post-tensioned bars (Soudki, Rizkalla, & Daikiw, 1995). All three configurations were tested under reverse cyclic loading, and the two bonded connections were also tested monotonically. It was found that the deformation capacities of all the connections were very similar to mild steel connections; however, the energy dissipation capacities were only about one-half compared to that of mild steel. Debonding was found to avoid rupture of the post-tensioning steel, and more than double the deformation capacity compared to the bonded connections. However this also resulted in a reduction in strength and stiffness.

Unbonded post-tensioning walls have several advantages over bonded reinforcement (post-tensioned and regular steel): the use of unbonded bars results in uniform strain in steel, therefore the yielding of the steel is delayed or prevented; since the bars are unbonded they do not transfer significant tensile stresses to the concrete, thus reducing cracking; it allows for gap openings along the horizontal joint with little to no damage occurring to the wall; and the restoring force of the post-tensioning steel results in a self-centering capability upon unloading, therefore residual displacements at the end of a severe earthquake are small (Y. Kurama, Pessiki, Sause, & Lu, 1999). However, these walls lack the energy dissipation capabilities of bonded connections, and therefore

require the addition of bonded mild steel reinforcement across the horizontal joint; such walls are called “hybrid walls”.

Hybrid walls have been shown to have greater energy dissipation capabilities compared to that of regular un-bonded post-tensioned walls, increasing up to four times when providing 0.75 times the amount of steel used in a comparable emulative wall (Y. C. Kurama, 2002). The addition of mild steel also decreases the maximum lateral displacement of the wall, and causes the response of the wall to decay faster, which subsequently reduces the number of large displacement peaks (Holden, Restrepo, & Mander, 2003; Y. C. Kurama, 2002; Restrepo & Rahman, 2007; Smith, Kurama, & McGinnis, 2013). The bonding of the mild steel for hybrid walls is achieved similarly to emulative walls, through either grouted splice sleeves, or grouted dowels (Restrepo & Rahman, 2007). Thus, in the application of hybrid walls, significant consideration is required in the secondary connection of the mild steel reinforcement.

2.3.2 Grouted Splice Sleeves

Grouted splice sleeves, also known as mechanical splices, achieve continuity by splicing bars end-to-end in short lengths through large confinement stresses. Commercially available grouted splice sleeves are common, but except basic evaluation reports, little relevant research is available on their behaviour (Jansson, 2008).

The first use of non-proprietary pipe splices was proposed by Einea et al. (1995). They tested four different splice sleeve configurations and reported that an embedment length as short as seven times the bar diameter was capable of developing the bar. They reported that regular steel pipe could generate a high level of confinement to the grout, preventing tensile splitting failures and achieving high bond strength.

Further research by Einea et al. (1999) investigated a splice connection consisting of steel spirals and multiple smaller lapping bars to splice the larger main bar. Different numbers of lap bars were tested (one, two, and four), with two lap bars performing the best and further tested. It was found that the steel spirals generated confinement similarly to transverse reinforcement, and allowed the bars to be developed in just seven times the bar

diameter. An equation was derived to determine the required development length based on a 95% confidence value. It was compared with the ACI 318-95 code equation and the equation proposed by Darwin et al. (1996). The ACI and the Darwin et al. (1996) equations were shown to overestimate the required development length by at least 76%, and 28%, respectively.

Many other researchers have investigated the application of grouted splice sleeves with the aim of creating simple, efficient, non-proprietary splice sleeves. Most splice sleeves consist of a thick walled steel pipe, but utilize different configurations to enhance bond, for instance via welded bars (Ling, Ahmad, Ibrahim, & Hamid, 2012), tapering the pipe diameter, bolts (Sayadi, Rahman, Jumaat, Johnson Alengaram, & Ahmad, 2014), steel rings, steel spirals (Hosseini et al., 2015), internal threading (Henin & Morcou, 2015), grout keys, or combinations of the aforementioned (Ling et al., 2014). All these splice sleeves generated high confinement stresses resulting in large bond stresses, which allowed them to develop the bars in very short embedment lengths ($6d_b$ to $8d_b$). Although these splices performed well, they require extensive fabrication (welding, threading, etc.) and have very poor construction tolerances. For these reasons, many precast manufacturers avoid them and prefer using grouted dowels.

2.3.3 Grouted Dowels

The grouted dowel connection works as a non-contact lap splice, where longitudinal bars protruding from the precast wall are grouted into corrugated metal ducts in the mating wall. Adjacent to the ducts are two bars that are used to lap splice the protruding bar into the mating wall, as illustrated earlier in **Fig. 2.1b**. The CPCI Design Manual recommends the duct diameter to be at least three times the reinforcing bar diameter to provide sufficient construction tolerances and ease the erection of the walls (CPCI, 2007). Bleeding of the grout can occur at the top of the duct, which can lower the mechanical properties of the grout. Thus, a minimum distance of 75 mm is left between the end of the bar and the top of the duct.

The grouted dowel connection method is used in a variety of precast connections including: columns, walls, beam-column connections, and bridge bent caps. Research is

available demonstrating the satisfactory use of this connection under full-scale seismic testing. However, sparse research is available on the bond of this connection, specifically, a reliable equation to accurately predict the required development length is yet to be developed.

Raynor et al. (2002) elaborated upon previous research on the development of a precast concrete framing system able to resist seismic loads and outperform conventional cast-in-place moment frames, referred to as a hybrid frame (Priestley et al., 1999; Stone, Cheok, & Stanton, 1995). The hybrid frame uses a combination of unbonded post-tensioned steel and bonded mild steel, both of which pass through ducts in the beams and columns, similar to the hybrid wall discussed earlier. The bonded steel bars are debonded in the beam at a specified length to prevent premature fracture due to high strain concentration at the beam-column interface. A finite element model was developed to generate a reliable equation to predict the required unbonded length. Since the results were proprietary to the company sponsoring the work, much data was withheld, and only the results of the bond stress-slip model were published. This makes it difficult for researchers to use/compare test results for future work. Furthermore, fiber-reinforced grout was used in this study, which is not typical of wall panel connections; further testing should be done with the desired grout type since it can play a significant role on the bond behaviour of the connection.

The design of lightly reinforced precast concrete wall panels for use in low-rise buildings subjected to high seismicity has previously been examined (Crisafulli, Restrepo, & Park, 2002). The wall-foundation connection consisted of a bed of dry-pack grout and two 16 mm diameter dowels with embedment lengths equal to $43d_b$ grouted into 50.8 mm (2 in.) diameter corrugated ducts. This structural system was found to be suitable for use in low-rise buildings with an abundance of wall panels subjected to high seismicity. The wall panels can be lightly designed and experience minimal structural damage since the plasticity concentrates at the connection region and is unable to spread through the wall panel. Although the performance of the connection was deemed satisfactory, the embedment length ($43 d_b$) was likely oversized; strain measurements taken along the

connecting bar found peak strains develop at the connection and decrease nearly linearly over $20 d_b$ once the yield strength is reached.

The use of grouted dowel connections for a precast bridge bent cap system was investigated by Steuck et al. (2009). A total of 14 pullout tests were conducted on bars with varying sizes and embedment lengths, with or without the addition of polypropylene fiber reinforcement. A non-linear finite element model was developed and used to establish a design equation to predict the required development length for this connection. It was found that this new equation requires a development length of $6.5 d_b$, while the ACI 318-05 equation 12-1 requires a development length of $20 d_b$. The ACI equation appears to be grossly conservative for this connection, requiring a development length three times greater than what was found in this research. However, the test setup was done to replicate a bridge bent cap system, using a much larger concrete block (914 mm diameter) than a wall connection would require. This extra concrete will affect the connection since it provides greater confinement effects. Additionally, this research focused on large diameter bars ($d_b = 32$ mm, 43 mm, and 57 mm) with a larger duct diameter/bar diameter ratio (3.6). Typical wall panel connections use 25 mm diameter bars with a duct diameter/bar diameter ratio of 3.0. For this reason, further testing is required to replicate the connections intended use.

More recently, this connection method has been examined for use in column-to-foundation connections subjected to high seismicity (Belleri & Riva, 2012; Popa, Papurcu, Cotofana, & Pascu, 2015). Belleri and Riva (2012) tested and compared the grouted dowel connection to cast-in-place and pocket-foundation connections. The grouted dowel connection performed exceptionally well, with the damage localized to the grout layer between the column and foundation, creating a simpler repair than that for cast-in-place concrete or pocket foundations. High ductility of the connection related to the confining effect of the corrugated sleeves was noticed; the high level of confinement also prevented the reinforcement from buckling. Popa et al. (2015) compared grouted dowel connections to cast-in-place concrete and had similar findings to that of Belleri and Riva (2012), noting that the cast-in-place specimen dissipated more energy, but also had more severe damage than that of the precast specimen. In both studies, it was concluded

that the grouted dowel connection is sufficient for use in a column-foundation connection subjected to high seismicity. However, in both cases the connection length was designed similarly to a reinforcing bar in concrete, likely overestimating the required embedment length.

The reinforcing bars in the grouted dowel connection behave differently than bars cast into regular reinforced concrete due to the confining effect of the duct (Belleri & Riva, 2012; Raynor, Dawn, & Stanton, 2002). Currently, the required development length is calculated as a regular reinforcing bar in concrete. This greatly underestimates the bond strength of this connection, since it does not accurately account for the confinement effects generated by the corrugated duct. The peak bond stress is much higher than that of reinforced concrete having comparable compressive strength, and the required embedment length can be reduced below requirements of the current standards (Raynor et al., 2002; Steuck et al., 2009). It has been reported that a well-confined connection can be overestimated by as much as 97% by the ACI code equation (Einea et al., 1999); therefore, further testing should be carried out to accurately predict the required embedment length for this grouted dowel connection.

2.4 Cold Weather Curing of Concrete

A major advantage of precast concrete construction is that it can continue throughout the winter much easier than cast-in-place concrete construction. However, an integral part of the precast wall panel assembly is the grouted dowel connection, which requires the placement of fresh cementitious grout to create the desired emulative connection. The effect of early-age exposure of this connection to subfreezing conditions is still largely unexplored. Therefore, to obtain an adequate background for a better understanding, a review of current literature on the cold weather curing of concrete is presented.

2.4.1 Effect on Compressive Strength

The effects of the curing temperature on the compressive strength gain for different cement Types (I, II, and III) with and without accelerators was studied by Klieger (1958). Without the use of accelerators, specimens cured at -4°C had significantly lower early-age strengths than that of specimens cured at ambient temperature (23°C), achieving

13%, 26%, and 70% of the 28 day strengths for cement Types II, I, and III, respectively. However, when accelerating admixtures were used, the concrete performed much better, gaining 56%, 66%, and 88%, of the 28 day strengths for cement Types II, I, and III, respectively. Furthermore, after 28 days, when the -4°C concrete was exposed to moist ambient conditions it reached or exceeded the long-term (3 months and 1 year) strength of the corresponding control concrete continuously cured at ambient conditions.

To determine the feasibility of concrete construction in the Arctic Sea, Aitcin et al. (1985) initially cured concrete at 4°C for 3 to 15 hours, and then placed it inside seawater at a temperature of 0°C until testing. It was observed that as the initial curing period increased, the compressive strength increased; and that the design strength of the concrete could be achieved if it was initially cured for a minimum of 9 hours at 4°C before being exposed to the 0°C seawater. The 28 and 56-day strengths were comparable to, and in some cases exceeded, that of concrete cured under room temperature conditions. The internal temperatures of the specimens were monitored, and it was found that due to the small specimen size, the concrete had reached the seawater temperature very rapidly. Although the temperature was cold, it remained above freezing, which could affect the degree of hydration significantly.

Gardner and Poon (1976) tested the mechanical properties of Type I and Type III cement concretes cured at low temperatures. The specimens were initially cured at 22°C for either 1, 3, or 7 days, before curing continued at 22°C, 13°C, and 2°C. The results showed that prolonged ambient curing increased compressive strength at early ages, but had negligible effect after 7 days. This implies that relatively low temperature curing had no detrimental effects on the long-term compressive strength.

Gardner et al. (1988) expanded on this work by curing concretes made with Type I and Type III cements at varying w/c ratios (0.35, 0.45, and 0.55) in 0°C ocean water. Their results indicated that the 0°C curing was only detrimental to the compressive strength at a w/c ratio of 0.55. In fact, the Type III cement cured at 0°C outperformed the ambient specimens after 7 days for a w/c ratio of 0.35, and after 14 days for a w/c ratio of 0.45. It

was concluded that the maturity method was not valid for concrete cured at cold temperatures.

Later work by Gardner (1990) showed that curing concrete made with Type I and Type I/fly ash cement concretes at 0°C had adverse effects on the compressive strength for w/c ratios of 0.35 and 0.55. The rate of strength gain was significantly slowed down for both concretes. This contradicts earlier work which determined that no adverse effects were observed when curing at 2°C (Gardner & Poon, 1976) and 0°C (Gardner, Sau, & Cheung, 1988).

Marzouk and Houssein (1995) investigated the effect of early-age exposure to cold ocean water on the mechanical properties of high-strength concrete containing silica fume and fly ash. They initially cured the concrete at ambient conditions for either 1, 14, or 28 days before exposing it to ocean water tanks at varying temperatures (20, 10, 0, -5, and -10°C). The specimens initially cured for 14 and 28 days were negligibly affected by the subfreezing exposure. The compressive strength, tensile strength, and modulus of rupture of the concrete specimens cured for 1 day continued to increase after exposure to subfreezing conditions, however, at a much slower rate than specimens cured at 20°C. At 7 days, the concretes cured at -5°C, and -10°C achieved 81% and 73% of that of the control cured for 7-day at ambient conditions, respectively. While at 28 days, the concretes cured at -5°C, and -10°C reached 78% and 69% of the strength of the control concrete cured for 28 days at ambient conditions, respectively. This research demonstrates that early-age subfreezing exposure had adverse effects on the compressive strength of high-strength concrete, with lower subfreezing temperatures resulting in lower compressive strength gain (Marzouk & Hussein, 1995). However, the subfreezing exposure did not halt the strength gain, and still resulted in maximum strengths of 52.2 MPa, and 47.4 MPa, for -5°C, and -10°C, respectively. The maturity method was found to reliably predict the compressive strength gain of most specimens. However, it was found to be inaccurate for specimens exposed to subfreezing temperatures after 1 day of initial curing.

Husem and Gozutok (2005) compared the effects of low temperature curing (10, 5, 0, -5°C) on the compressive strength of ordinary and high-performance concrete. The high-performance concrete incorporated fly ash and silica fume, and had lower w/c ratio than that of ordinary concrete (0.30 compared to 0.50, respectively). Specimens were cured for 7 days at the specified temperature, and then re-exposed to ambient conditions until 28 days. The high-performance concrete performed much better than the ordinary concrete, especially at lower temperatures; however, both concretes suffered significant reductions in strength when cured below freezing. For the -5°C curing, the high-performance concrete had a 63% reduction in strength at 7 days, while the ordinary concrete had a 79% reduction.

Nassif and Petrou (2013) found that concrete specimens cured at -5°C achieved 50% of the 28-day strength of their counterpart concrete cured at 20°C. This strength gain was largely attributed to the heat of hydration raising the internal temperature above freezing for three days. However, in their study, relatively larger volumes of concrete were cast (750x750x300 mm slabs) than what is typically used for the grouted dowel connections. Thus, it is unlikely that the heat of hydration will significantly raise the internal temperature of the grouted dowel connections above freezing for up to three days, allowing further strength gain to occur.

It has been shown that concrete can gain compressive strength when exposed to subfreezing temperatures at early ages; though the rate of strength gains and overall strengths are typically much lower when compared to that at ambient curing conditions. Yet, concrete can continue to hydrate once re-exposed to ambient conditions and can reach, or even surpass, the long-term compressive strength of concrete continuously cured at ambient conditions. However, from the literature presented herein, it is evident that the rate of strength gain is very dependent on the concrete mix constituents and proportions, with some researchers having contradictory results for similar mixes. Therefore, it is important to accurately test the desired mix under appropriate conditions that mimic the expected field situation.

2.4.2 Effect on Bond Strength

Data from several studies examining the effect of cold temperatures on concrete bond behaviour has been compiled and examined (Huang, Chang, Shih, & Lee, 1989). The studies encompassed a temperature range of -10°C to -70°C , and included both normal and high-strength concrete. The authors normalized the bond stress, u_b , and slip, s , to the maximum bond stress, u_{max} , and corresponding maximum slip, $s_{u_{max}}$, and plotted u_b/u_{max} versus $s/s_{u_{max}}$ for six specimens with different compressive strengths. They determined that the temperature had little influence on the bond behaviour, and that it is mainly dependent on the concrete compressive strength. It was also found that the relationship between bond strength and the square root of compressive strength of concrete remained linear at subfreezing temperatures.

Another concern with the early-age exposure to subfreezing temperatures is that frost damage due to trapped internal water may occur and affect the overall bond behaviour of the connection. However, a study examining the effect of freeze-thaw damage on concrete bond has shown that even in cases where freeze-thaw damage occurred, the bond strength remained proportional to the square root of the compressive strength of concrete (Shih, Lee, & Chang, 1988).

The bond behaviour of concrete at low temperatures remained essentially the same as at normal temperatures, with the bond strength remaining proportional to the square root of the compressive strength of concrete when exposed to subfreezing temperatures (Gardner & Poon, 1976; Huang et al., 1989), even when frost damage occurred (Shih et al., 1988). Since the bond strength has been shown to be approximately proportional to the square root of the compressive strength of concrete, a reduction in the compressive strength of the concrete due to cold weather curing will not affect the bond strength as greatly. For example: if the concrete achieves only 80% of the desired compressive strength, it still achieves ~89.4% of the desired bond strength. However, this relationship needs to be investigated for this particular connection and specific grout mixture. From the above discussion of relevant research in the open literature, it can be expected that the grouted dowel connection will continue to gain some strength when exposed to subfreezing

temperatures at early-age. However, due to the complexity and variable nature of concrete, dedicated testing and quantitative assessment is needed.

2.5 References

- ACI Committee 318. (2014). Building Code Requirements for Structural Concrete (ACI 318-14) and Commentary (ACI 318R-14). *American Concrete Institute*. Farmington Hills, MI.
- ACI Committee 408. (2003). Bond and Development of Straight Reinforcing Bars in Tension (ACI 408-03). *American Concrete Institute*. Farmington Hills, MI, USA.
- ACI Committee 550. (2009). Guide to Emulating Cast-in-Place Detailing for Seismic Design of Precast Concrete Structures (ACI 550-09). *American Concrete Institute*. Farmington Hills, MI, USA.
- Aitcin, P.-C., Cheung, M. S., & Shah, V. K. (1985). Strength Development of Concrete Cured Under Arctic Sea Conditions. *Temperature Effects on Concrete*. ASTM International.
- Belleri, A., & Riva, P. (2012). Seismic performance and retrofit of precast concrete grouted sleeve connections. *PCI Journal*, 57(1), 97–109.
- CPCI. (2007). CPCI Design Manual. *Canadian Precast/Prestressed Concrete Institute*. Ottawa, ON.
- Crisafulli, F. J., Restrepo, J. I., & Park, R. (2002). Seismic Design of Lightly Reinforced Precast Concrete Rectangular Wall Panels. *PCI Journal*, 47(4), 104–121.
- Darwin, D., Zuo, J., Tholen, M. L., & Idun, E. K. (1996). Development length criteria for conventional and high relative rib area reinforcing bars. *ACI Structural Journal*, 93(3), 347–359.
- Einea, A., Yamane, T., & Tadros, M. K. (1995). Grout-filled pipe splices for precast concrete construction. *PCI Journal*, 40(1), 82–93.
- Einea, A., Yehia, S., & Tadros, M. K. (1999). Lap splices in confined concrete. *ACI Structural Journal*, 96(6), 947–955.
- Gardner, N. J. (1990). Effect of Temperature on the Early-Age Properties of Type I, Type III, and Type I/ Fly Ash Concretes. *ACI Materials Journal*, 87(1), 68–78.
- Gardner, N. J., & Poon, S. M. (1976). Time and Temperature Effects on Tensile Bond, and Compressive Strengths. *ACI Journal Proceedings*, 73(7), 405–409.
- Gardner, N. J., Sau, P. L., & Cheung, M. S. (1988). Strength development and durability of concretes cast and cured at 0 C. *ACI Materials Journal*, 85(6), 529–536.
- Henin, E., & Morcou, G. (2015). Non-proprietary bar splice sleeve for precast concrete construction. *Engineering Structures*, 83, 154–162.
- Holden, T., Restrepo, J., & Mander, J. B. (2003). Seismic Performance of Precast Reinforced and Prestressed Concrete Walls. *Journal of Structural Engineering*, 129(3), 286–296.

- Hosseini, S. J. A., Rahman, A. B. A., Osman, M. H., Saim, A., & Adnan, A. (2015). Bond behavior of spirally confined splice of deformed bars in grout. *Construction and Building Materials*, 80, 180–194.
- Huang, X. P., Chang, K. C., Shih, T. S., & Lee, G. C. (1989). Analytical Models of Local Concrete-Steel Bond at Low Temperature. *Journal of Cold Regions Engineering*, 3(4), 159–171.
- Husem, M., & Gozutok, S. (2005). The effects of low temperature curing on the compressive strength of ordinary and high performance concrete. *Construction and Building Materials*, 19(1), 49–53.
- Hutchinson, R. L., Rizkalla, S. H., Lau, M., & Heuvel, S. (1991). Horizontal Post-Tensioned Connections for Precast Concrete Loadbearing Shear Wall Panels. *PCI Journal*, 36(6), 64–76.
- Jansson, P. (2008). Evaluation of Grout-Filled Mechanical Splices for Precast Concrete Construction. *Michigan Department of Transportation*. Lansing, Michigan.
- Klieger, P. (1958). Effect of mixing and curing temperature on concrete strength. *ACI Journal*, 54(6), 1063–1081.
- Kurama, Y. C. (2002). Hybrid post-tensioned precast concrete walls for use in seismic regions. *PCI Journal*, 47(5), 36–59.
- Kurama, Y., Pessiki, S., Sause, R., & Lu, L.-W. (1999). Seismic Behavior and Design of Unbonded Post-Tensioned Precast Concrete Walls. *PCI Journal*, 44(3), 72–89.
- Ling, J. H., Ahmad, A. B., & Ibrahim, I. S. (2014). Feasibility study of grouted splice connector under tensile load. *Construction and Building Materials*, 50, 530–539.
- Ling, J. H., Ahmad, A. B., Ibrahim, I. S., & Hamid, Z. A. (2012). Behaviour of grouted pipe splice under incremental tensile load. *Construction and Building Materials*, 33, 90–98.
- Marzouk, H., & Hussein, A. (1995). Effect of Curing Age on High-Strength Concrete at Low Temperatures. *Journal of Materials in Civil Engineering*, 7(3), 161–167.
- Moosavi, M., Jafari, A., & Khosravi, A. (2005). Bond of cement grouted reinforcing bars under constant radial pressure. *Cement and Concrete Composites*, 27(1), 103–109.
- Nassif, A. Y., & Petrou, M. F. (2013). Influence of cold weather during casting and curing on the stiffness and strength of concrete. *Construction and Building Materials*, 44, 161–167.
- Orangun, C. O., Jirsa, J. O., & Breen, J. E. (1977). A Reevaluation of Test Data on Development Length and Splices. *Journal of the American Concrete Institute*, 74(3), 114–122.
- Popa, V., Papurcu, A., Cotofana, D., & Pascu, R. (2015). Experimental testing on emulative connections for precast columns using grouted corrugated steel sleeves. *Bulletin of Earthquake Engineering*, 13(8), 2429–2447.

- Priestley, M. J. N., Sritharan, S., Conley, J. R., & Pampanin, S. (1999). Preliminary Results and Conclusions From the PRESSS Five-Story Precast Concrete Test Building. *PCI Journal*, 44(6), 42–67.
- Raynor, D. J., Dawn, E. L., & Stanton, J. F. (2002). Bond-Slip Response of Reinforcing Bars Grouted in Ducts. *ACI Structural Journal*, 99(5), 568–576.
- Restrepo, J. I., & Rahman, A. (2007). Seismic Performance of Self-Centering Structural Walls Incorporating Energy Dissipators. *Journal of Structural Engineering*, 133(11), 1560–1570.
- Sayadi, A. a., Rahman, A. B. A., Jumaat, M. Z. Bin, Johnson Alengaram, U., & Ahmad, S. (2014). The relationship between interlocking mechanism and bond strength in elastic and inelastic segment of splice sleeve. *Construction and Building Materials*, 55, 227–237.
- Shih, T. S., Lee, G. C., & Chang, K. C. (1988). Effect of Freezing Cycles on Bond Strength of Concrete. *Journal of Structural Engineering*, 114(3), 717–726.
- Smith, B. J., Kurama, Y. C., & McGinnis, M. J. (2013). Behavior of Precast Concrete Shear Walls for Seismic Regions: Comparison of Hybrid and Emulative Specimens. *Journal of Structural Engineering*, 139(11), 1917–1927.
- Soroushian, P., Choi, K., Park, G., & Aslani, F. (1991). Bond of deformed bars to concrete: effects of confinement and strength of concrete. *ACI Materials Journal*, 88(3), 227–232.
- Soudki, K. A., Rizkalla, S. H., & Daikiw, R. W. (1995). Horizontal Connections for Precast Concrete Shear Walls Subjected to Cyclic Deformations Part 2: Prestressed Connections. *PCI Journal*, 40(5), 82–96.
- Steuck, K. P., Eberhard, M. O., & Stanton, J. F. (2009). Anchorage of large-diameter reinforcing bars in ducts. *ACI Structural Journal*, 106(4), 506–513.
- Stone, W. C., Cheok, G. S., & Stanton, J. F. (1995). Performance of hybrid moment-resisting precast beam-column concrete connections subject to cyclic loading. *ACI Structural Journal*, 92(2), 229–249.
- Untrauer, R. E., & Henry, R. L. (1965). Influence of Normal Pressure on Bond Strength. *ACI Journal*, 62(5), 577–586.

3 INVESTIGATION OF GROUTED DOWEL CONNECTIONS FOR PRECAST CONCRETE WALL PANELS¹

3.1 Introduction

Precast concrete construction has become more popular since the 1980's when the precast seismic structural system (PRESSSS) research program began. The conclusion of the research showed that precast concrete structural systems can perform as well, and in some cases better, than cast-in-place concrete (Priestley et al., 1999). Precast concrete load bearing wall panels are commonly used in medium- and high-rise buildings due to their cost-effectiveness, ease and speed of erection, and high quality control achieved at the manufacturing plant. However, an integral part of this structural system that needs particular attention is the connection since it directly affects the structure's strength and stability.

As discussed in Chapter 2, designers prefer to use emulative connections rather than jointed connections as they perform similarly to a cast-in-place structure, and can therefore be designed similarly. The two most common methods of achieving emulative wall panel connections are through mechanical splices, sometimes referred to as grouted splices, and the grouted dowel connection. There is much research demonstrating the feasibility of these grouted splices (Einea et al., 1995; Jansson, 2008; Ling et al., 2014). However, they generally have poor construction tolerances and are costly due to the laborious fabrication required.

In the grouted dowel connection, a reinforcing bar protruding from the lower wall panel is grouted into a corrugated duct cast into the upper wall panel as shown in **Fig. 1.1** and **Fig. 2.1b**. This connection is preferred due to its simplicity, favourable construction tolerances, and cost effectiveness. In this system, the grouted dowel carries the tensile forces across the wall panel connection. Since ductility is required in this system, these

¹ A version of this chapter was submitted for publication as: Provost, D. J., Elsayed, M., & Nehdi, M. L., "Investigation of Grouted Dowel Connections for Precast Wall Construction." *Submitted to ACI Structural Journal, November 2016.*

dowels are required to undergo yielding, similar to regular reinforced concrete. Although there are specific code requirements for the use of mechanical splices, there are none for the use of reinforcing bars grouted into ducts, and research on this connection is sparse.

Raynor et al. (2002) tested the use of this connection type for a hybrid frame system. They examined the bond-deformation relationship of the connection and concluded that it behaved differently than bars in regular reinforced concrete. For instance, peak bond stresses were found to be higher than those possible for comparable reinforced concrete, therefore allowing for shorter embedment lengths than required by current codes. They also observed different damage patterns compared to those in reinforced concrete. There was no visible cracking in the grout cylinder; instead there was significant grout crushing surrounding the reinforcing bar lugs. This behavior is different than that of bars in reinforced concrete, which usually exhibit extensive tensile radial bond cracks (Goto, 1971). It was concluded that the lack of visible cracking along with the obvious local grout crushing indicate that the duct provided sufficient confinement to prevent splitting or cracking failure. Since the results were proprietary to the company sponsoring the work, much data was withheld, including peak bond stresses and required development lengths; only the connection's bond-slip response was presented.

This connection was later examined for use in a precast bridge bent system (Steuck et al., 2009). The authors conducted a total of 14 pullout tests with varying bar sizes, embedment lengths, and the use of fiber reinforcement. Based on the experimental results, the following design equation (**Eq. 3.1**) was proposed to calculate the required development length.

$$l_d = \frac{f_y}{10.8\sqrt{f'_g}} d_b + \left(\frac{d_{duct} - d_b}{2} \right) \quad (3.1)$$

Where,

l_d = development length (mm);

f_y = yield strength of the bar (MPa);

f'_g = grout compressive strength (MPa);

d_b = bar diameter (mm);

d_{duct} = duct diameter (mm).

This equation was found to produce development lengths three times smaller than that required by ACI 318-05 equation 12-1. However, this research considered only large diameter bars (32 mm to 57 mm) with larger duct diameter/bar diameter ratios of 3.6, whereas a typical wall panel connection usually uses a 25M bar with a duct diameter/bar diameter ratio of 3.0. This design equation was also developed with only 55 MPa (8000 psi) strength grout, and may not be accurate with lower grout strengths.

For most cast-in-place reinforced concrete members, a tensile splitting failure is the most common bond failure mode exhibited. Current design codes require the development length of this connection to be designed as a regular bar in normal reinforced concrete (ACI Committee 318, 2014). Since this design equation is based upon test results for bar splices in concrete, which typically fail through tensile splitting, it predicts much lower bond stresses and consequently much longer embedment lengths than required for reinforcing bars grouted into ducts. Researchers have demonstrated that this can lead to greatly oversized embedment lengths when this failure mode is suppressed or delayed, allowing much larger bond stresses to be generated (Einea et al., 1999).

It has been shown that the grouted dowel connection is quite different than regular bar in reinforced concrete. However, since limited research is available on this connection, it is not well known which parameters will influence the connections behavior. The studies that have so far examined the bond behavior of this connection for uses in hybrid frames (Raynor et al., 2002) and precast bridge bent cap systems (Steuck et al., 2009) have used larger concrete covers (127 mm [5 in.], and 356 mm [14 in.], respectively) than that typically encountered in precast concrete wall panels (64 mm [2.5 in.]). Furthermore, neither of these studies examined the effect of eccentric bar placement within the duct, or how the absence of the duct affects the behavior of the connection. Therefore, it is

important to replicate field conditions when testing grouted dowel connections in order to accurately estimate its strength for each particular application.

3.2 Research Significance

With the grouted dowel becoming a common connection method in precast concrete wall construction, there is need to acquire an enhanced understanding of the mechanics of this connection and accurately determine its bond strength. This chapter presents experimental results for the grouted dowel connection used in large-scale precast concrete wall panel assembly. Based on the experimental results obtained herein and relevant data published previously, a new design equation is proposed, which provides a basis for more accurately estimating both the bond strength and required development length for grouted dowel connections.

3.3 Experimental Program

3.3.1 Test Specimens and Setup

The test specimens were configured to represent a typical full-scale grouted dowel connection used in precast concrete wall panels. Each specimen used an unreinforced precast concrete block with a thin-walled corrugated steel duct concentrically placed in the block. The blocks were 203 x 203 mm (8 x 8 in.) in cross-section, and 406 mm (16 in.) tall; except for the specimens with embedment lengths of 36 bar diameters, which had a height of 914 mm (36 in.). The corrugated steel ducts had an internal diameter of 76 mm (3 in.) and a thickness of 0.36 mm (0.014 in.). The test specimen is portrayed in **Fig. 3.1**.

Unless otherwise stated, the test bars were grouted concentrically within the duct and extended 25 mm (1 in.) above the concrete block to measure slip during testing. To examine the effect of eccentric bar placement within the connection, test bars were placed directly against the edge of the duct and grouted. For specimens with no ducts present, a 76 mm (3 in.) diameter cylindrical void cast in the concrete block was grouted. Similar to field conditions, the grout was poured from the passive end of the connection. In typical field conditions, an additional 76 mm (3 in.) is grouted above the bar at the top end of the

duct to avoid the bleeding distance of the grout (Crisafulli et al., 2002). However, during grouting, care was taken to ensure no bleeding, and this distance was removed to allow easier measurements of bar slip at the top (passive) end.

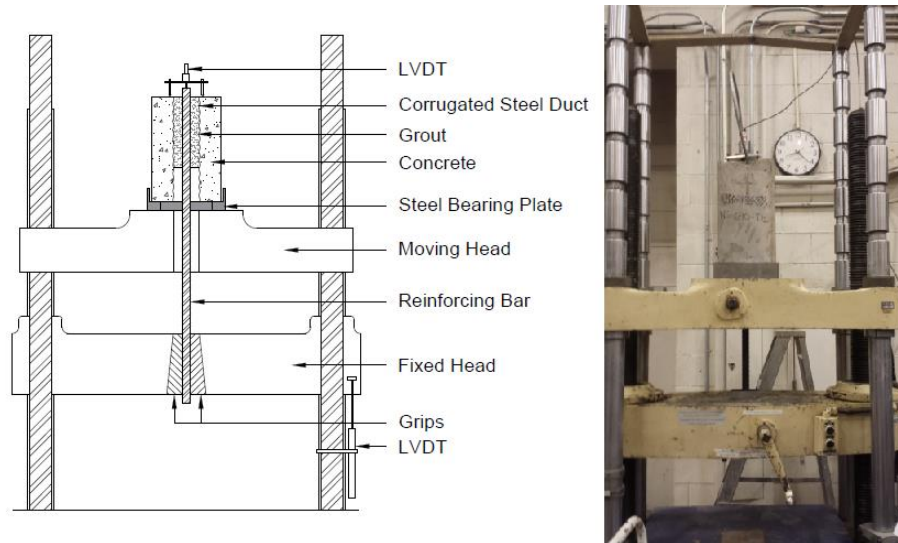


Figure 3.1: Pullout test specimen and setup.

In field construction, precast concrete wall panels are typically braced for one week. Hence, to mimic field conditions, the test specimens were tested at 7 days. Embedment lengths of 4, 6, 8, and 12 bar diameters were tested using a 25M bar to examine the bond behavior envelope (elastic and plastic behavior). A much longer embedment length of 36 bar diameters was also tested since this is a typical connection length used in practical applications. For each embedment length, two identical specimens were tested to examine the repeatability of results. The specimen notation is as follows ($lAB-n$), to indicate the embedment length ($l = 4, 6, 8, 12, \text{ or } 36$ bar diameters), bar placement ($A = C$ for concentric or E for eccentric), presence of the duct ($B = D$ for duct or N for no duct), and n represents the specimen number.

The concrete blocks were cast using self-consolidating concrete having an average compressive strength of 50.6 MPa (7340 psi). Commercially available non-shrink grout was used as per industrial practice, mixing one 25 kg bag with 3.75 L of water to achieve adequate fluid consistency. The average 7-day compressive strength of the grout was 38.4 MPa (5570 psi), measured on 3 replicate 76 x 152 mm (3 x 6 in.) cylinders. The duct

could not be accurately tested because disassembling it would result in plastic deformations, therefore altering its mechanical properties. The test bars used were 25M deformed steel with a specified yield strength of 400 MPa (58 ksi).

The pullout test setup is illustrated in **Fig. 3.1**. The test specimens were placed on a 216 x 216 mm (8.5 x 8.5 in.) steel bearing plate atop the active end of an open loop Tinius Olsen testing machine. The bearing plate had a square internal void that was used to distribute the load to a 25 mm wide outer edge of the concrete block so as to avoid inducing compression stresses in the bonded region, which is known to affect the bond behavior of the bar (ACI Committee 408, 2003). One strain based linear variable displacement transducer (LVDT) was placed on the unloaded end of the bar to measure slip. Another LVDT was attached to the testing machine crosshead, measuring its relative movement, which represents the bar elongation. The specimen was tested at a loading rate of 0.5 kN/s.

3.4 Experimental Results and Discussion

The results of the eighteen pullout specimens are summarized in **Table 3.1**. Current design codes require mechanical splices to develop 125% of the bars yield strength to account for material over-strength and ensure that the bar yields (ACI Committee 318, 2014). The same criterion was used herein, and referred to as the strength ratio, R_s .

$$R_s = \frac{f_s}{f_y} \quad (3.2)$$

A strength ratio exceeding 1.25 was reached with an embedment length of 8 bar diameters. At an embedment length of 12 bar diameters (305 mm [12 in.]) – the shortest allowable embedment length according to ACI 318-14 – the bar approached its ultimate stress, reaching an average of 679 MPa (98.5 ksi). The degree of bar yielding appears to have an effect on the bond stress; at an embedment length of 12 bar diameters, the bar had undergone most yielding, approaching fracture, yet had the lowest recorded bond stress. Steuck et al. (2009) also observed a similar trend and attributed it to the inelastic elongation of the bar which reduced the effective cross-sectional area, partially

disengaging the bar from the grout, and therefore reducing the bond capacity. However, further testing should be carried out to accurately quantify this effect.

Table 3.1: Pullout test results

Specimen	P , kN (kip)	f_s , MPa (ksi)	u_{eff} , MPa (psi)	s_{max} , mm (in.)	R_s	Failure Mode
4CD-1	111.1 (25.0)	226 (32.8)	18.3 (2650)	0.65 (0.03)	0.57	Bar Pullout
4CD-2	124.3 (27.9)	253 (36.7)	20.4 (2960)	0.83 (0.03)	0.63	Bar Pullout
6CD-1	161.4 (36.3)	329 (47.7)	15.9 (2310)	0.29 (0.01)	0.82	Bar Pullout
6CD-2	182.4 (41.0)	372 (53.9)	18.0 (2610)	0.58 (0.02)	0.93	Bar Pullout
8CD-1	252.6 (56.8)	515 (74.6)	17.8 (2580)	0.65 (0.03)	1.29	Bar Pullout
8CD-2	258.6 (58.1)	527 (76.4)	18.2 (2640)	0.65 (0.03)	1.32	Bar Pullout
12CD-1	342.4 (77.0)	698 (101.2)	15.4 (2230)	1.12 (0.04)	1.74	Bar Pullout
12CD-2	324.4 (72.9)	661 (95.8)	14.6 (2110)	0.59 (0.02)	1.65	Bar Pullout
12CN-1	230.2 (51.8)	469 (68.0)	10.3 (1500)	0.63 (0.02)	1.17	Tensile Splitting
12CN-2	234.5 (52.7)	478 (69.3)	10.5 (1530)	0.30 (0.01)	1.19	Tensile Splitting
12ED-1	299.2 (67.3)	610 (88.4)	13.4 (1950)	0.35 (0.01)	1.52	Bar Pullout
12ED-2	302.5 (68.0)	616 (89.4)	13.6 (1970)	0.40 (0.02)	1.54	Bar Pullout
12EN-1	232.0 (52.2)	473 (68.5)	10.4 (1509)	0.43 (0.02)	1.18	Tensile Splitting
12EN-2	194.2 (43.7)	396 (57.4)	8.7 (1260)	0.21 (0.01)	0.99	Tensile Splitting
36CD-1	324.1 (72.9)	660 (95.8)	4.6 (660)	0.00	1.65	Bar Fracture
36CD-2	326.6 (73.4)	665 (96.5)	4.6 (670)	0.00	1.66	Bar Fracture
36ED-1	312.8 (70.3)	637 (92.4)	4.4 (640)	0.00	1.59	Bar Fracture
36ED-2	313.7 (70.5)	639 (92.7)	4.4 (640)	0.000	1.60	Bar Fracture

3.4.1 Failure Modes

Specimens with an embedment length of 12 bar diameters or less and grouted concentrically within the corrugated steel duct all failed through bar pullout due to shearing of the surrounding grout. Hairline cracking of the concrete block was observed in some of these specimens as shown in **Fig. 3.2a**; however, it did not appear to affect the connection's capacity. This cracking can be prevented by reinforcing the concrete block, and is unlikely to occur in practical applications due to the reinforcement already present. The ability of this connection to nearly achieve the ultimate bar stress while suffering minimal cracking indicates that this connection could be used with a clear concrete cover of as low as 64 mm (2.5 in.) for 50 MPa (7300 psi) concrete.

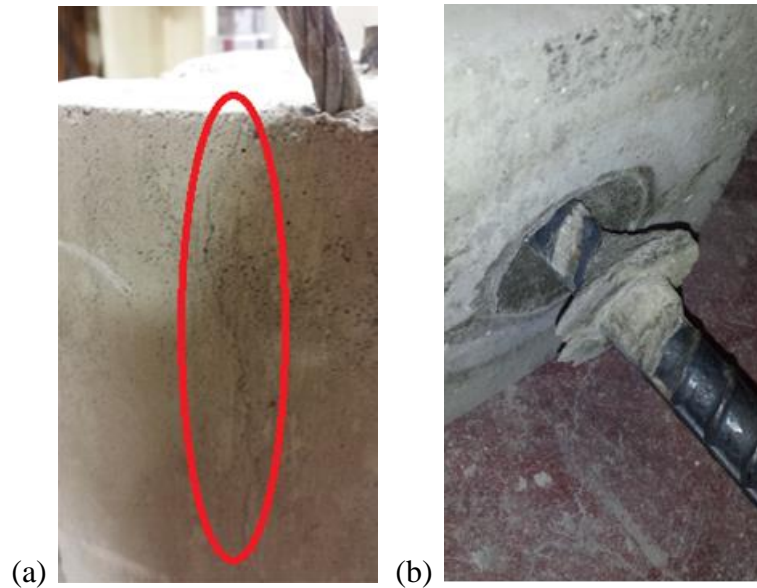


Figure 3.2: Specimen damage: a) hairline cracking of concrete block; b) grout conical failure.

Conical grout failures at the free surface were also observed for all specimens (**Fig. 3.2b**). This failure can be attributed to Goto cracks, which form cones at the bar lugs near the free ends of concrete for reinforcing bars projecting from concrete and placed in tension (Goto, 1971). The presence of this failure at an oversized embedment length of 36 bar diameters confirms that it is based on the boundary conditions, and not due to other bond parameters. Goto (1971) originally observed such cracks to have angles of $\alpha = 45$ to 80 degrees to the bar axis, with most being approximately $\alpha = 60$ degrees. This failure mode was also observed by Steuck et al. (2009), who recorded cracks producing angles of $\alpha = 45$ to 60 degrees from the bar axis. In the present study, the cone varied between $\alpha = 30$ to 60 degrees, and in some specimens, the cone followed the spiral lug as shown in **Fig. 3.2b**. It is important to note that some applications of this connection require the bar to be debonded at the free surface to prevent premature fracture (Raynor et al., 2002); in such a case the conical failure described above will not be present.

Specimens with an embedment length of 36 bar diameters all experienced failures due to bar fracture. Bar fracture is the preferred failure mode since it allows the bar to fully develop, therefore offering a higher tensile capacity of the connection; and causing larger

bar displacement due to post-yielding bar elongation, ensuring more ductile behavior of the connection. However, for the purpose of accurately quantifying the bond strength of this connection, a pullout due to bond failure is desirable, which is the rationale for exploring shorter embedment lengths in the present study.

3.4.2 Effect of Duct

Researchers investigating grouted splices have argued that the thick-walled steel cylinders act as passive confinement, generating large confinement stresses, which increase the bond strength of the reinforcing bar (Einea et al., 1995; Ling et al., 2012). It is believed that the grouted dowel connection explored in the present study would behave similarly; however, it relies on the stiffness of the surrounding concrete, whereas grouted splices have sufficient stiffness of their own. Steuck et al. (2009) reported no ducts yielding and found that the ducts contribute rather negligibly to the total hoop stiffness compared to the surrounding concrete cylinder. This passive confinement suppresses the expansive tensile splitting failure that normally occurs in regular reinforced concrete, allowing a shearing pullout bond failure to occur instead.



Figure 3.3: Splitting expansion failure of corrugated duct.

The low duct stiffness was also observed in preliminary testing, where the present authors tested the grouted duct without surrounding concrete. The duct split open through tensile splitting expansion of the grout (**Fig. 3.3**) at around 100 kN, which is a significantly lower force than that required to fully develop a 25 mm diameter reinforcing bar. This

was also observed by Ling et al. (2014) who tested a similar grouted duct for use as a splice sleeve, failing at very low load.

Even though the duct has insufficient strength to develop the bar alone, its use is paramount for the connection to function properly. The primary role of the duct is to provide adequate bond between the surrounding precast concrete and the freshly placed grout. However, the duct does also help to confine the surrounding concrete, preventing it from a tensile splitting failure. In the absence of the corrugated duct, two additional failure modes can occur: the entire grout sleeve can pull out from the surrounding concrete; or the concrete can experience a tensile splitting failure. **Figure 3.4** displays the failure mode of specimen 12CN-2, where the grout sleeve began to slip before the surrounding concrete failed through tensile splitting. These failure modes are conflict with findings of researchers who previously investigated bars grouted into concrete (Darwin & Zavaregh, 1996). This is likely due to the difference in the size of the grouted cavity; since for a 25 mm diameter bar, Darwin and Zavaregh (1996) used 32 mm (1.25 in.) holes, while the current research used 76 mm (3 in.) holes.



Figure 3.4: Tensile splitting failure of the concrete block for specimen 12CN-2.

The reduction in strength due to the absence of the corrugated steel duct can be observed in **Fig. 3.5**. This chart displays the ratios of failure loads for specimens with no duct and/or cast with eccentricity to the average failure load of control specimens 12CD-1 and 12CD-2. When the duct was absent from specimens grouted concentrically (specimens

12CN-1 and 12CN-2), there was a 30% reduction in the connection's strength. This is due to the lack of confinement, therefore causing the surrounding concrete block to fail through tensile splitting. For instance, in specimen 12CN-1, the tensile cracking split through the grout cylinder as shown in **Fig. 3.6**.

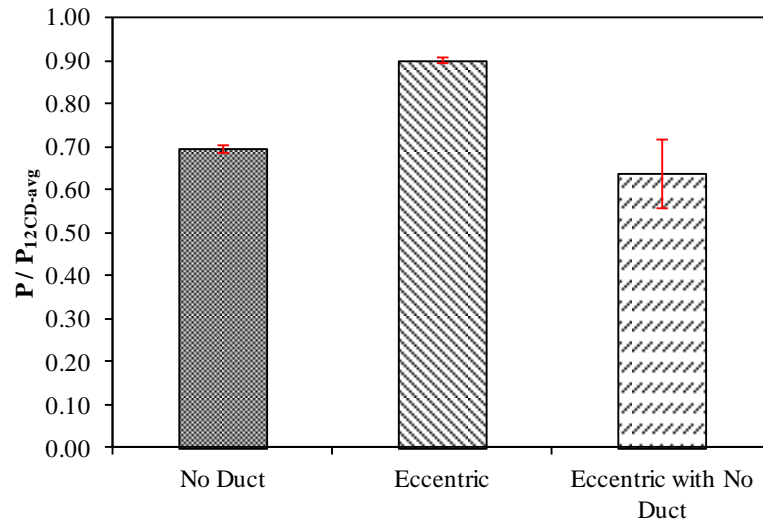


Figure 3.5: Reduction in strength due to absence of duct and/or eccentricity.



Figure 3.6: Tensile splitting through grout cylinder of specimen 12CN-1.

3.4.3 Effect of Eccentricity

Specimens grouted eccentrically within ducts experienced a pullout failure as described earlier. However, these specimens achieved lower bond stresses when compared to concentrically grouted control specimens. This was apparently due to the extensive tensile cracking of the surrounding concrete block (**Fig. 3.7**). Unlike specimen 12CN-1 in which cracks occurred in the surrounding concrete and grout (**Fig. 3.6**), the tensile cracking in specimens 12ED-1 and 12ED-2 only occurred in the surrounding concrete, but not in the duct or grout. This suppression of tensile cracking is attributed to the confining effect of the duct. This tensile cracking reduced the stiffness and subsequently the confinement effect of the surrounding concrete. As discussed earlier, the large bond stress achieved by this connection is dependent upon the high confinement effect. Therefore, this reduction in confinement led to a reduction in strength by about 10% as shown in **Fig. 3.5**. When the bars are aligned eccentrically against the duct wall, the connection generates greater concentrated tensile stresses in the surrounding concrete, leading to the extensive tensile cracking displayed in **Fig. 3.7**.



Figure 3.7: Tensile splitting of surrounding concrete for specimen 12ED-1.

Eccentric bar placement had a relatively small effect on longer connection lengths in which specimens experienced bar fracture. When specimens with an embedment length of 36 bar diameters were tested, eccentric specimens still failed through bar fracture, though about 4% reduction in strength was recorded. It is inconclusive whether the

eccentric bar placement affects the connection in the absence of the duct; specimen 12EN-1 (eccentric with no duct) performed similarly to both specimens 12CN-1 and 12CN-2 (no duct but concentric). Yet, specimen 12EN-2 had a reduction in strength of 16% due to eccentricity, and an overall reduction of 42% due to a combined effect of the absence of duct and eccentricity. Specimen 12EN-2 also had a very brittle failure through tensile splitting of both the grout and surrounding concrete (**Fig. 3.8**).



Figure 3.8: Tensile splitting of grout and surrounding concrete for specimen 12EN-2.

3.4.4 Bond Behaviour

For the purpose of accurately determining the bond strength of this grouted dowel connection, only specimens that experienced bar pullout due to bond failure will be further examined. These specimens are reported in **Table 3.2** with their normalized strength data. The higher bond stresses associated with this connection are attributed to the pullout failure due to shearing of the surrounding grout, as opposed to a splitting failure in reinforced concrete which occurs at much lower loads. Since the grout cone near the free surface did not contribute to the shearing failure plane (**Fig. 3.2**), and may have occurred before failure (Goto, 1971), its length is not included when calculating the effective bond stress, u_{eff} (**Eq. 3.3a**). This assumption is confirmed by specimens tested in Chapter 4, where comparable bond stresses were reached with bars that were wrapped at the free surface, therefore prohibiting a conical grout failure.

$$u_{eff} = \frac{P \times 10^3}{\pi \cdot d_b \cdot l_{eff}} \quad (3.3a)$$

Where,

$$l_{eff} = l_{emb} - \left(\frac{d_{duct} - d_b}{2 \tan(\alpha)} \right) \quad (3.3b)$$

With a constant duct diameter of $3d_b$, and assuming an average angle of 45 degrees,

$$l_{eff} = l_{emb} - d_b \quad (3.3c)$$

Where,

u_{eff} = effective bond stress (MPa);

P = load (kN);

l_{eff} = effective embedment length (mm);

d_b = bar diameter (mm);

d_{duct} = duct diameter (mm);

α = grout cone angle, degrees.

Table 3.2: Normalized strength data

Specimen	l_{eff}/d_b	P , kN (kip)	$f_s/\sqrt{f'_g}$, $\sqrt{\text{MPa}} (\sqrt{\text{psi}})$	$u_{eff}/\sqrt{f'_g}$, $\sqrt{\text{MPa}} (\sqrt{\text{psi}})$
4CD-1	4	111.1 (25.0)	36.5 (440)	2.95 (35.5)
4CD-2	4	124.3 (27.9)	40.9 (492)	3.30 (39.7)
6CD-1	6	161.4 (36.3)	53.1 (639)	2.57 (30.9)
6CD-2	6	182.4 (41.0)	60.0 (722)	2.90 (35.0)
8CD-1	8	252.6 (56.8)	83.0 (1000)	2.87 (34.6)
8CD-2	8	258.6 (58.1)	85.0 (1020)	2.94 (35.4)
12CD-1	12	342.4 (77.0)	113 (1360)	2.48 (29.8)
12CD-2	12	324.4 (72.9)	107 (1280)	2.35 (28.3)

The bar stress-displacement behavior corresponding to each dowel embedment length experiencing pullout failure is displayed in **Fig. 3.9**. The recorded displacement is the relative movement of the testing machine’s crossheads; this therefore accounts for both slip and bar elongation. For all specimens, the behavior mimicked that of a regular steel bar until the peak load was reached, then a steep drop in load was observed, followed by a more gradual decrease in load until the test was stopped. The criterion for stopping the test was once a slip of ~8mm was reached since it envelopes the entire bond-slip response.

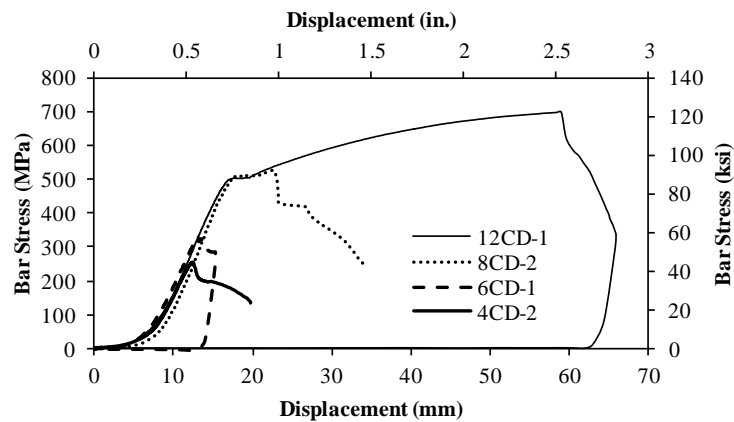


Figure 3.9: Bar stress-displacement plots for each embedment length.

Previous research has reported that the average bond stress is directly proportional to the square root of the concrete compressive strength (Untrauer & Henry, 1965). Therefore, to accurately analyze and compare the bond strengths and bond-slip behavior, the effective bond strength, u_{eff} , was normalized with the square root of the grout compressive strength, $\sqrt{f_g'}$. The normalized bond stress-slip behavior is similar for all embedment lengths, with small differences in peak bond stress and corresponding slip (**Fig. 3.10**). However, this is rather common in pullout tests, due to the variable nature of concrete materials (Eligehausen, Popov, & Bertero, 1983).

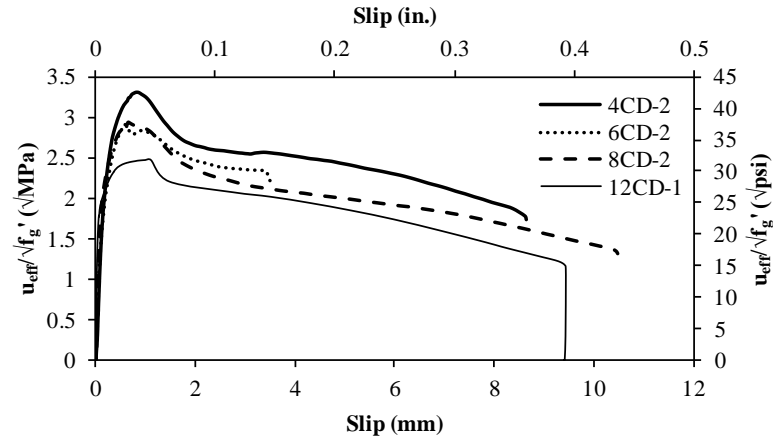


Figure 3.10: Normalized bond stress-slip response for each embedment length.

The normalized bond stress-slip relationship was defined by fitting curves to the experimental data for an embedment length of 8 bar diameters, which represents the average response for all tested specimens. The corresponding equations are:

$$u_{eff} / \sqrt{f'_g} = 0.66 \ln(s) + 3.3 \quad 0 \leq s \leq 0.6 \quad (3.4a)$$

$$u_{eff} / \sqrt{f'_g} = 2.96 \quad 0.6 \leq s \leq 1.0 \quad (3.4b)$$

$$u_{eff} / \sqrt{f'_g} = 3.70 - 0.743s \quad 1.0 \leq s \leq 1.7 \quad (3.4c)$$

$$u_{eff} / \sqrt{f'_g} = 2.66 - 0.128s \quad 1.7 \leq s \leq 10.5 \quad (3.4d)$$

Where,

$$u_{eff} / \sqrt{f'_g} = \text{normalized effective bond stress } (\sqrt{\text{MPa}});$$

$$s = \text{slip (mm)}.$$

The normalized bond stress-slip model developed herein had most variability with specimen 4CD-2 with a mean squared error of 0.12. However, comparing model

predictions to experimental results of specimen 8CD-2, which represents the average response for all tested specimens, it had a mean squared error of 0.014. The normalized bond stress-slip model is shown in **Fig. 3.11** and compared to previously established bond models by Raynor et al. (2002) and Steuck et al. (2009) for bars grouted in ducts, and by Eligehausen et al. (1983) for regular reinforced concrete. The differences are apparent, with each bond model representing bars grouted in ducts predicting much larger bond stresses than the model for reinforced concrete. This is due to the aforementioned confinement effect of the duct.

The model developed by Raynor et al. (2002) predicts a much higher bond stress than the other models. This may be attributed to differences in testing; in the present study and in Steuck et al. (2009), the load was distributed to the outer edge of the concrete to prevent inducing additional compressive stresses affecting the bond behavior. Conversely, in Raynor et al. (2002), the concrete block was actually bolted to the test frame with steel bearing plates, which may have induced confinement stresses increasing the bond capacity. However, the differences in bond stress between the current model, and the model proposed by Steuck et al. (2009) are small, and within the scatter of the test results as can be observed in **Fig. 3.12**.

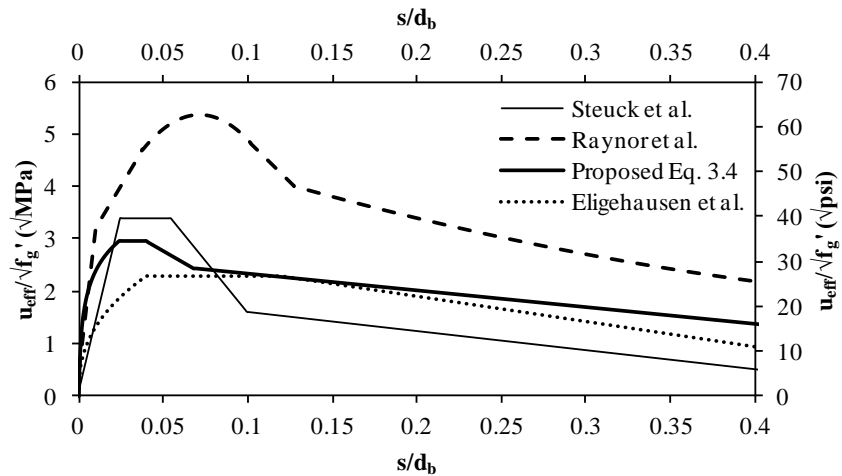


Figure 3.11: Comparisons of current bond-slip models.

3.4.5 Analysis of Experimental Results

The tensile bar stress versus embedment length results from the tests conducted in the present study were plotted and compared with the results from Steuck et al. (2009). Initially the results from Steuck et al. (2009) appeared to have higher stresses for similar embedment lengths. However, once the bar stress was normalized with the square root of the compressive strength of grout, the difference disappeared (**Fig. 3.12**). This suggests that the duct diameter/bar diameter ratio only affects the effective length of the bar, and not the overall strength.

It can be observed in **Fig. 3.12** that the normalized tensile stress varies approximately linearly with the normalized embedment length. This indicates that the maximum bond stress was approximately constant in all tests, with the exception of one specimen that fractured in the testing by Steuck (2009). A design equation (**Eq. 3.5**) was derived by fitting a lower bound 99% confidence curve to the data.

$$l_d = \frac{f_y}{9.6\sqrt{f'_g}} d_b + \left(\frac{d_{duct} - d_b}{2} \right) \quad (3.5)$$

Where,

l_d = development length (mm);

f_y = yield strength of the bar (MPa);

f'_g = grout compressive strength (MPa);

d_b = bar diameter (mm);

d_{duct} = duct diameter (mm).

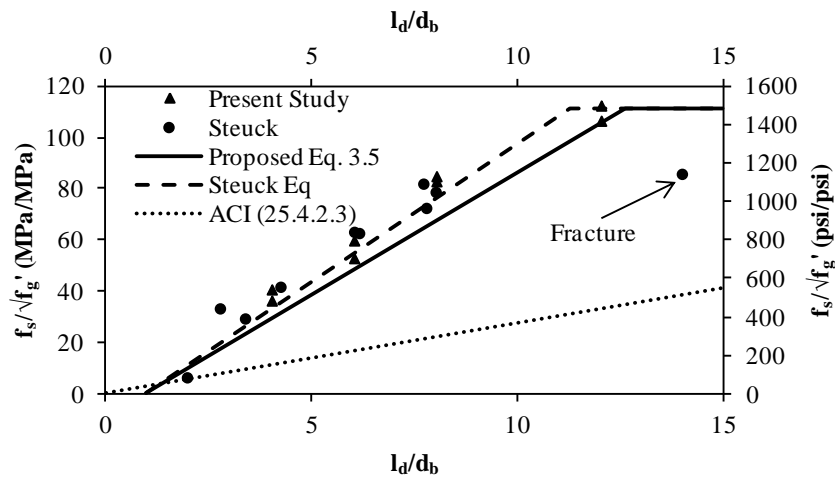


Figure 3.12: Normalized bar stress versus normalized embedment length.

The proposed design equation shares the same material variables as **Eq. 3.1** by Steuck et al. (2009), while accounting for lower strength grouts, resulting in desirably more conservative design. As can be observed in **Fig. 3.12**, the design equation crosses the embedment length axis at approximately 1.0; this represents the conical failure of the grout which as mentioned, does not contribute to the bond strength. This is accounted for in the design equation through the second term, and should be ignored when debonding of the bar is present. This design equation is applicable for duct diameter/bar diameter ratios of 3.0-3.6 using non-shrink grouts only; the use of different grout types has not been investigated herein, and thus needs to be validated for specific use in this particular connection. The data from Steuck et al. (2009) had a maximum grout compressive strength of 70 MPa. Therefore, the proposed design equation should be limited to 70 MPa until such data on using higher strength grouts becomes available.

3.5 Comparisons with Current Design Equations

A graphical comparison of **Eq. 3.1**, **Eq. 3.5**, and the ACI 318-14 equation (25.4.2.3) is shown in **Fig 3.12**. It can be observed that the ACI equation greatly underestimates the axial bar stress for any embedment length. The equation developed by Steuck et al. (2009) fits the data well; however, it overestimates the stress of some specimens, displaying its lack of conservatism. Conservative design is rather required for such a

connection involving various uncertain parameters. A comparison of the predicted bar stress from **Eq. 3.5** versus experimental peak bar stress for the present data, and data from Steuck et al. (2009) is displayed in **Fig. 3.13**, where anything under the line results in a conservative design. It can be observed that the proposed equation does not overestimate any of the experimental data; rather it conservatively under predicts the bar stress. While this requires slightly longer development lengths, it allows for a desirable conservative level of safety necessary in design.

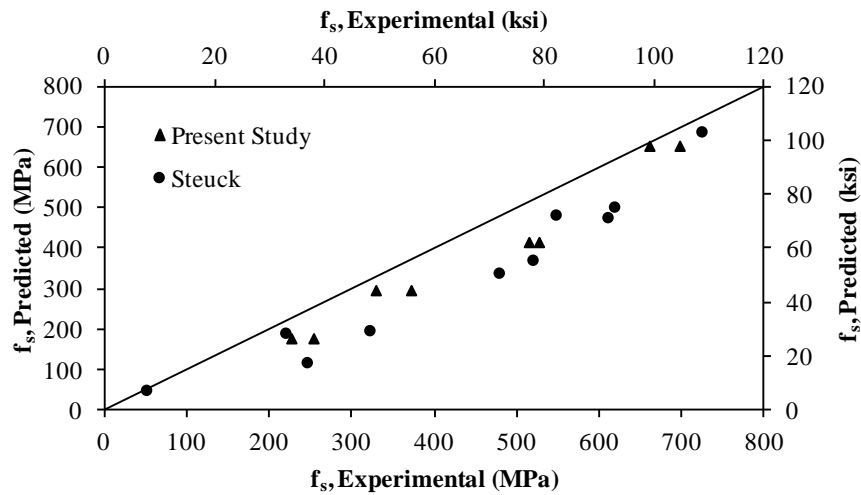


Figure 3.13: Predicted versus experimental peak bar stress comparison.

Assuming a specified steel yield strength of 420 MPa, grout compressive strength of 35 MPa, and a duct diameter of $3d_b$, the proposed design equation (**Eq. 3.5**) results in an embedment length of $8.4d_b$. The current ACI 318-14 equation (25.4.2.3) greatly overestimates this length, resulting in a development length 3.08 times larger than required. The current ACI code does not account for the higher confinement generated by the presence of the duct. This was also observed by Einea et al. (1999) who used spirals to generate greater confinement effects than in regular concrete; they found that the ACI equation overestimated the required length by almost double.

Since **Eq. 3.1** developed by Steuck et al. (2009) predicts higher bar stresses, it tends to underestimate the required length. For the same properties mentioned above, **Eq. 3.1** only

provides 90% of the calculated required length. The equation proposed in the present study is 10% more conservative than **Eq. 3.1** for all grout strengths. An accurate relationship between cyclic and monotonic load could not be found for this connection. However, Steuck et al. (2009) suggested a conservative factor of 1.5 for determining the seismic development lengths. Therefore, the development length of this equation for use in seismic applications would approximately be $12.6d_b$.

3.6 Future Research

The present study provides a comprehensive investigation on the use of the grouted dowel connection in precast wall construction under monotonic loading. However, an accurate relationship between monotonic and cyclic loading has yet to be established, and requires further attention. Full-scale testing of the connection under flexural loading should also be examined to determine the effect of combined shear and tension stresses.

3.7 Summary and Conclusions

Eighteen pullout tests were performed on a grouted dowel connection used in large-scale precast concrete wall panel construction. The experimental results were compared to relevant data in the open literature in order to develop an accurate equation for predicting the development length which accounts for the effect of bar size, steel strength, and grout compressive strength. The results were also compared to the current ACI 318-14 equation (25.4.2.3), and the equation developed by Steuck et al. (2009). The following conclusions can be drawn from this study:

1. This grouted dowel connection can be used with a clear concrete cover of as low as 64 mm (2.5 in.) for 50 MPa (7300 psi) concrete.
2. The steel duct creates a higher confinement effect than present in regular reinforced concrete, allowing for a shear pullout failure rather than a tensile splitting failure.
3. This failure mode occurs at significantly higher bond stresses, allowing for a reduction in required embedment length.

4. The absence of the duct can reduce the strength of this connection by about 30%.
5. Eccentric bar placement generates tensile stress concentrations in the surrounding concrete, reducing the strength by about 10% for embedment lengths of 12 bar diameters, and by about 4% for embedment lengths of 36 bar diameters.
6. The current ACI equation (25.4.2.3) does not account for the greater confinement effect of the duct, therefore greatly overestimates the required development length.
7. The equation proposed in the present study requires development lengths of $8.4d_b$ for yield, and $13.1d_b$ for bar fracture, assuming that a 35 MPa grout is used.
8. The equation proposed by Steuck et al. (2009) is not sufficiently conservative, which is a disadvantage for designing the grouted dowel connection since safety is necessary considering the high variability of concrete materials and the many exogenous variables that can affect its performance. The equation proposed in the present study is 10% more conservative than the equation proposed by Steuck et al. (2009), which is a desirable feature in design applications.
9. The equation proposed in the present study is applicable for non-shrink grouts having a compressive strength up to 70 MPa. Using other grout types has not been investigated herein, and thus needs to be validated for specific use in this particular connection. The use of higher strength grouts (>70 MPa) has also not been explored, and therefore the proposed design equation should be limited to 70 MPa until such data on using higher strength grouts becomes available.

3.8 References

- ACI Committee 318. (2014). Building Code Requirements for Structural Concrete (ACI 318-14) and Commentary (ACI 318R-14). *ACI 318-14*. Farmington Hills, MI.
- ACI Committee 408. (2003). Bond and Development of Straight Reinforcing Bars in Tension Reported by ACI Committee 408. *ACI 408-03*. Farmington Hills, MI, USA.
- Crisafulli, F. J., Restrepo, J. I., & Park, R. (2002). Seismic Design of Lightly Reinforced Precast Concrete Rectangular Wall Panels. *PCI Journal*, 47(4), 104–121.

- Darwin, D., & Zivaregh, S. S. (1996). Bond Strength of Grouted Reinforcing Bars. *ACI Structural Journal*, 93(4), 486–495.
- Einea, A., Yamane, T., & Tadros, M. K. (1995). Grout-filled pipe splices for precast concrete construction. *PCI Journal*, 40(1), 82–93.
- Einea, A., Yehia, S., & Tadros, M. K. (1999). Lap splices in confined concrete. *ACI Structural Journal*, 96(6), 947–955.
- Eligehausen, R., Popov, E. P., & Bertero, V. V. (1983). Local bond stress-slip relationships of deformed bars under generalized excitations. *Report No. UCB/EERC-83/23*. Earthquake Engineering Research Center, University of California-Berkeley.
- Goto, Y. (1971). Cracks Formed in Concrete Around Deformed Tension Bars. *ACI Journal Proceedings*, 68(4), 244–251.
- Jansson, P. (2008). Evaluation of Grout-Filled Mechanical Splices for Precast Concrete Construction. *Michigan Department of Transportation*. Lansing, Michigan.
- Ling, J. H., Ahmad, A. B., & Ibrahim, I. S. (2014). Feasibility study of grouted splice connector under tensile load. *Construction and Building Materials*, 50, 530–539.
- Ling, J. H., Ahmad, A. B., Ibrahim, I. S., & Hamid, Z. A. (2012). Behaviour of grouted pipe splice under incremental tensile load. *Construction and Building Materials*, 33, 90–98.
- Priestley, M. J. N., Sritharan, S., Conley, J. R., & Pampanin, S. (1999). Preliminary Results and Conclusions From the PRESSS Five-Story Precast Concrete Test Building. *PCI Journal*, 44(6), 42–67.
- Raynor, D. J., Dawn, E. L., & Stanton, J. F. (2002). Bond-Slip Response of Reinforcing Bars Grouted in Ducts. *ACI Structural Journal*, 99(5), 568–576.
- Steuck, K. P., Eberhard, M. O., & Stanton, J. F. (2009). Anchorage of large-diameter reinforcing bars in ducts. *ACI Structural Journal*, 106(4), 506–513.
- Untrauer, R. E., & Henry, R. L. (1965). Influence of Normal Pressure on Bond Strength. *ACI Journal*, 62(5), 577–586.

4 EARLY-AGE EXPOSURE OF GROUTED PRECAST CONCRETE WALL CONNECTIONS TO SUBFREEZING CURING TEMPERATURES¹

4.1 Introduction

In cold climates, subfreezing temperatures can prevail for long periods of time, which can significantly slow or halt concrete construction. The ACI Committee 306R-10 defines cold weather as a period of three or more successive days when the average daily air temperature drops below 4°C and does not exceed 10°C for more than one-half of any 24-h period (ACI Committee 306, 2010). Concrete must reach a compressive strength of 3.5 MPa before exposure to subfreezing temperatures; failure to do so will result in significant reduction of both the strength and stiffness of the concrete. Winter construction of cast-in-place concrete requires the heating of large areas for extended periods of time, and typically includes the use of accelerating admixtures to ensure the development of adequate compressive strength. However, such methods can significantly increase cost, while making it difficult to maintain superior quality control.

A major advantage of precast concrete construction is that it can continue throughout adverse weather conditions, including cold weather, since the structural elements are cast and cured in a quality controlled precast plant. However, the grouted dowel connection (**Fig. 1.1, 2.1b**) requires the in-situ placement of fresh grout. In cold weather construction, the entire floor is blanketed and heated during grout mixing and pouring. Usually, the heating is stopped after one day, and the connection is exposed to subfreezing temperatures, before the grout is fully cured. This could affect the bond strength of the connection, and possibly the overall structural integrity.

¹ Parts of this chapter were published or submitted as: Provost, D. J., Elsayed, M., & Nehdi, M. L., (2016) “Investigation of Grouted Precast Concrete Wall Connections at Subfreezing Conditions,” *Proceedings of the CSCE 5th International Materials Specialty Conference*, London, ON, MAT-719, and Provost, D. J., Elsayed, M., & Nehdi, M. L., “Early-age Exposure of Grouted Precast Concrete Wall Connections to Subfreezing Curing Temperatures,” *submitted to Construction and Building Materials Journal, November 2016*.

The authors could not retrieve any studies in the open literature examining the effect of subfreezing curing conditions on the bond strength of grouted dowel connections. However, Gardner and Poon (1976) investigated the effect of 2°C curing on the bond strength of concrete, and concluded that the bond strength was affected proportionally to the square root of the compressive strength, irrespective of the temperature or cement type. Most existing research work has focused on the effect subfreezing exposure on the compressive strength, since the latter is used in the ACI (2014) equation (25.4.2.3) to determine the bar development length.

Results of several studies generally indicate that the compressive strength gain of concrete was adversely affected by early-age exposure to subfreezing temperatures. For instance, Klieger (1958) found that curing concrete at -4°C resulted in significantly lower 28-day compressive strengths by 13% and 70%, for concretes made with Type I and Type III cements, respectively. Gardner (1990) showed that curing concrete at 0°C had adverse effects on the compressive strength of concrete, contradicting earlier work which determined that no adverse effects were observed when cured at 2°C (Gardner & Poon, 1976) and 0°C (Gardner et al., 1988). Furthermore, the magnitude of strength loss of concrete cured in cold weather varied significantly between studies. In two separate investigations, high-strength concrete incorporating silica fume and fly ash was cured in -5°C ocean water, resulting in 7-day strengths of 37% (Husem & Gozutok, 2005), and 81% (Marzouk & Houssein, 1990). Such inconsistent results demonstrate the importance of testing the actual grout mixture to be used in precast wall panel construction, while accurately replicating the subfreezing conditions to be experienced in the field.

4.2 Research Significance

Since a typical precast concrete wall structural system depends primarily on the performance of grouted dowel connections, it is crucial to understand how early-age exposure to subfreezing temperatures will affect the grout and the connection's bond strength. It has been widely accepted that the bond strength of concrete is directly proportional to the square root of its compressive strength (Untrauer & Henry, 1965), even at low temperature curing (Gardner & Poon, 1976) and in the case of frost damage (Shih et al., 1988). Since grouted dowel connections are used in a variety of precast

structures including beam-column joints in hybrid frames (Raynor et al., 2002) and bridge bent caps (Steuck et al., 2009), the research conducted herein on the effect of subfreezing exposure on grouted dowel connections could be extended to the winter construction of various precast structures such as buildings and bridges.

4.3 Experimental Investigation

Full-scale precast concrete wall panels are typically braced for one week. Hence, the focus of this study was on the properties of the grout in the first 7 days. The grout used in this study was a commercially available, pre-packaged, non-shrink grout containing well-graded fine aggregate and fly ash. One 25 kg bag was mixed with 3.75 L of water to achieve a fluid consistency with a specified 7-day compressive strength of 30 MPa, as indicated by the manufacturer. All materials were stored, cast, and cured at ambient laboratory conditions ($T = 23 \pm 1^\circ\text{C}$). After one day of curing at ambient conditions, the specimens were moved to a temperature-controlled environmental chamber preset at the specified temperature until the testing date. The internal temperatures of the grout cylinders and pullout specimens were monitored at subfreezing temperatures with probes carefully placed at the center of the cylinders and pullout specimens; temperature readings were taken every 10 minutes for 7 days. The control specimens were maintained at ambient laboratory conditions until testing. Since the fresh grout in this connection is encompassed by the wall panel, it is difficult to continuously moist-cure it in the field. Therefore, to replicate practical applications, the grout was not moist-cured.

The main temperatures examined in this study were -10°C and ambient ($T = 23 \pm 1^\circ\text{C}$). The mechanical properties of the grout including compressive strength, tensile strength, young's modulus, and bond strength were evaluated. Thermogravimetric analysis (TGA) was used to elucidate the effect of subfreezing curing on the grout's hydration products. Mercury intrusion porosimetry (MIP) tests were also performed to examine how the subfreezing curing affected the porosity and pore size distribution of the grout.

To determine the compressive strength of the grout, 75 x 150 mm (3 x 6 in.) cylinders were cast. The grout specimens were tested according to ASTM C39 (Standard Test Method for Compressive Strength of Cylindrical Concrete Specimens). Each reported

compressive strength result is the average value obtained on three identical specimens. The compressive strength gain of the grout was monitored at ambient ($T = 23 \pm 1^\circ\text{C}$), and at temperatures of 1°C , -10°C , and -20°C . The initial ambient curing time before exposure to subfreezing conditions was varied at 0, 8, and 12 hours. The grout was tested at ages of 1, 3, 5, and 7 days, for all curing regimes, and 28 days for curing at -10°C and ambient conditions.

The tensile strength of the grout was determined according to ASTM C496 (Standard Test Method for Splitting Tensile Strength of Cylindrical Concrete Specimens) using the average value of three identical 75 x 150 mm (3 x 6 in.) cylinders at each curing regime. The tensile strength gain of the grout was assessed at 1, 3, 7 days and at 28 days for curing at -10°C and ambient temperature.

The modulus of elasticity and Poisson's ratio of the grout were determined according to ASTM C469 (Test Method for Static Modulus of Elasticity and Poisson's Ratio of Concrete in Compression) using the average of two 100 x 200 mm (4 x 8 in.) identical cylinders. The modulus of elasticity was measured at 7 and 28 days for specimens cured at -10°C and ambient temperature.

Thermogravimetric analysis is commonly used to investigate the hydration of cementitious materials and the reactivity of pozzolans (Pinto, Büchler, & Dweck, 2007; Trník, Scheinherrová, Kulovaná, & Černý, 2016; Vedalakshmi, Raj, Srinivasan, & Babu, 2003). In this test, hydration is typically assessed in terms of the decomposition of the major hydration products such as calcium silicate hydrate (CSH), ettringite, and portlandite (CH) (Bhatty, 1991) at certain temperature levels. Fragments were taken from the internal sections of crushed grout cylinders used for testing the compressive strength of the grout, and were submersed in isopropanol to stop hydration reactions. The specimens were subsequently crushed by hand using a mortar and pestle, and then dried in a desiccator until a constant mass was reached. The samples were heated up to 1050°C at a heating rate of $10^\circ\text{C}/\text{min}$ in a nitrogen atmosphere with a flow rate of 40 ml/min.

Moreover, mercury intrusion porosimetry (MIP) tests were performed to determine the effect of early-age subfreezing curing on the porosity and pore size distribution of the

grout. Fragments were taken from the internal sections of crushed grout cylinders used for testing the compressive strength of the grout. Care was taken to ensure that these fragments were not fractured, and multiple tests were run to confirm the repeatability of the results. The specimens were immediately submerged in isopropanol to stop hydration reactions, and subsequently dried in a desiccator until a constant mass was reached. The tests were run using a Micrometrics AutoPore IV 9500 Series porosimeter having a range of pressures from 0 to 414 MPa (60,000 psi).

Furthermore, pullout test specimens were designed to represent typical grouted dowel connections used in full-scale precast concrete wall panel construction. Each pullout test specimen used an unreinforced precast concrete block with a thin-walled corrugated steel duct concentrically cast into the block. The concrete blocks were cast using self-consolidating concrete with an average compressive strength of 50.6 MPa (7340 psi), and had a cross-sectional area of 203 x 203 mm (8 x 8 in.) and a height of 406 mm (16 in.). The corrugated steel ducts had an internal diameter of 76 mm (3 in.) and a thickness of 0.36 mm (0.014 in.). The mechanical properties of the ducts could not be accurately tested since disassembling it would result in plastic deformations, therefore altering its engineering properties.

Deformed 25M steel bars were placed concentrically within the duct and grouted from the passive (top) end of the connection. The bars extended 25 mm (1 in.) above the concrete block to measure slip during testing. The top and bottom of the test bars were wrapped with plastic to de-bond sections of the bar so that the embedment length, l_d , would lie in the middle of the specimen. This de-bonding was done to avoid compression stresses induced from the pullout testing, which is known to affect the bond behavior of the bar (ACI Committee 408, 2003). The test reinforcing bars had a specified yield strength of 400 MPa.

The pullout test specimen and setup are illustrated in **Fig. 4.1**. After 7 days of curing, the specimens were placed on a 216 x 216 mm (8.5 x 8.5 in.) steel bearing plate atop the active pulling end of an open loop Tinius Olsen testing machine with a maximum capacity of 530 kN (119 kips). A 216 x 216 mm (8.5 x 8.5 in.) steel bearing plate with a

square internal void was used to distribute the load to a 25 mm wide outer edge of the concrete block to further help avoid compression stresses induced from the pullout test, as previously mentioned. One strain based linear variable displacement transducer (LVDT) with a 25 mm gauge length was placed on the unloaded end of the bar to measure slip. A second LVDT was used to measure the testing machine crosshead movement, which represents the bar elongation. The specimen was loaded monotonically in tension at a rate of 0.5 kN/s. The test was ended once either the test bar fractured, or the LVDT measuring slip reached its gauge length.

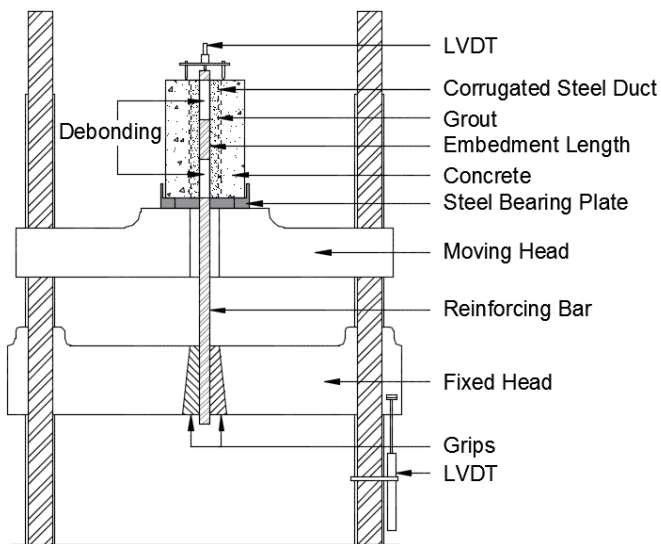


Figure 4.1: Pullout test specimen and setup.

4.4 Experimental Results and Discussion

4.4.1 Compressive Strength

The compressive strength of grout specimens cured under various temperature regimes are displayed in **Table 4.1**. Regardless of the severity of subfreezing conditions, the grout continued to develop mechanical strength after exposure to cold weather. It can be observed that a lower curing temperature resulted in lower compressive strength of the grout as expected, in agreement with previous studies examining the effect of cold weather curing of concrete (Gardner, 1990; Marzouk & Houssein, 1990). The grout specimens cured at 1°C performed the best, achieving 94% of the 7-day strength of

control specimens cured at ambient temperature. There appeared to be no significant difference between the results of grout specimens cured at -10°C or -20°C, with both curing conditions yielding about 84% of that of the control specimens. When the grout specimens were exposed to ambient temperatures subsequent to sub-freezing curing for an additional 28 days, it began to gain strength once more, achieving 97% of that of the control. The compressive strength development for all tested temperature curing regimes was fitted using regression analysis as plotted in **Fig. 4.2**. It was found that the strength development of the grout at all temperatures followed a logarithmic function; $f_g' = a + b \ln(t)$; where, f_g' = compressive strength of the grout in MPa; t = time in days, and a , b = regression constants.

Table 4.1: Compressive strength of grout at various curing temperatures

	Age (Days)	Ambient (23°C)	1°C	-10°C	-10°C (12 h)	-10°C (8 h)	-20°C
f_g' (MPa)	1	19.18	21.56	20.55	4.88 ^a	0 ^b	21.99
	3	33.75	30.42	26.72	9.85	1.95	30.19
	5	36.64	34.89	32.32	11.02	3.27	32.29
	7	38.43	35.99	32.51	11.41	3.54	32.34
	28	39.31	-	32.58	-	-	-
	7+28*	-	-	37.26	-	-	-

Note: * After 7-days grout was re-exposed to ambient temperature for 28 days.

^a Tested at 12 hours. ^b Tested at 8 hours.

The internal temperature of the grout specimens cured at subfreezing conditions are presented in **Fig. 4.3**. The figure was truncated at 3 days since no change in temperature was observed up until testing at day 7. All temperature recordings were taken on 75 x 150 mm (3 x 6 in.) cylinders unless otherwise stated. Due to the small specimen size, the internal temperature of the grout reached the external subfreezing temperature very rapidly; this has also been reported in previous studies (Aitcin, Cheung, & Shah, 1985). Some researchers argue that the heat of hydration causes the internal temperature of the concrete to remain above freezing to allow hydration to proceed (Nassif & Petrou, 2013). However, as observed in **Fig. 4.3**, such an effect was not observed herein. The relatively larger pullout specimen took 2.5 hours longer to reach freezing temperature compared to the smaller cylindrical specimens due to an insulation effect of the concrete surrounding

the grout. Yet, this time difference is unlikely to lead to significant additional strength gain.

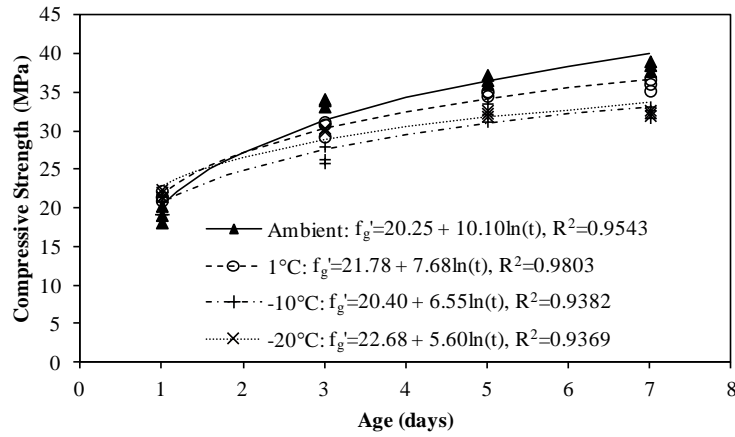


Figure 4.2: Compressive strength development for various temperatures.

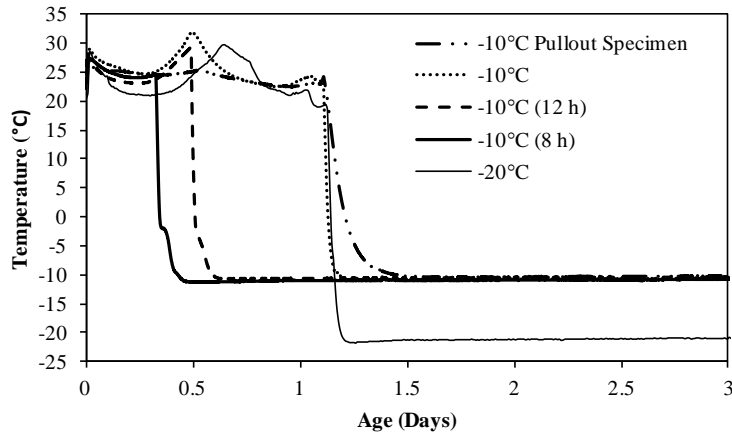


Figure 4.3: Internal grout temperature for varying subfreezing conditions.

4.4.1.1 Initial Curing Period

Grout specimens that were placed in the environment chamber at -10°C immediately after casting achieved no significant strength after 7 days of curing. The grout could easily be pulled apart by hand, indicating that cement hydration reactions were inhibited.

Grout specimens that were allowed to cure at ambient conditions for 8 hours before exposure to subfreezing temperatures achieved 7-day compressive strength of 3.5 MPa.

The specimens were tested at 8 hours before exposure to subfreezing temperature inside the environmental chamber and achieved zero compressive strength. Examining the internal temperatures from **Fig. 4.3**, it can be observed that the specimen initially cured for 8 hours followed a similar trend to that of specimens initially cured for 1 day at ambient conditions. At 8 hours when it was placed inside the environmental chamber, its internal temperature was about to begin increasing due to the exothermic cement hydration reactions. The initial and final setting times of the grout are 4 hours and 6.5 hours, respectively. The lack of internal temperature increase, along with the zero strength achieved at 8 hours, were indications that the specimen just achieved final set, and that cement hydration reactions which produce mechanical strength were just beginning.

When the grout was allowed to cure for 12 hours [at ambient temperature](#) before exposure to subfreezing temperatures, it achieved a 7-day compressive strength of 11.4 MPa. At 12 hours, the grout had achieved a compressive strength of 4.9 MPa before being placed inside the environmental chamber at -10°C . Specimens initially cured for 12 hours at ambient temperature performed better than those initially cured for only 8 hours because they experienced significant cement hydration reactions before subfreezing exposure. This can be observed in **Fig. 4.3**, where the specimens initially cured for 12 hours experienced a steady increase in internal temperature, approaching the peak temperature of the specimens cured for 1 day, before being placed inside the environmental chamber. Again, this increase in internal temperature is attributed to the progress of exothermic cement hydration reactions.

The ratio of compressive strength at varying initial ambient curing periods to the 7-day strength of identical specimens initially cured for 1 day is displayed in **Fig. 4.4**. It can be observed that the compressive strength continued to increase up to 7 days for all curing conditions, with the specimens initially cured for 12 hours greatly outperforming those cured for only 8 hours. Yet, both types of specimens incurred large reduction in compressive strength of 65% and 89%, for 12 hours and 8 hours initial curing, respectively, when compared to specimens initially cured at ambient temperature for 1 day. This emphasizes the importance of the initial curing period before early-age

exposure of the grout to subfreezing temperatures, in agreement with previous research (Aitcin et al., 1985; Gardner & Poon, 1976).

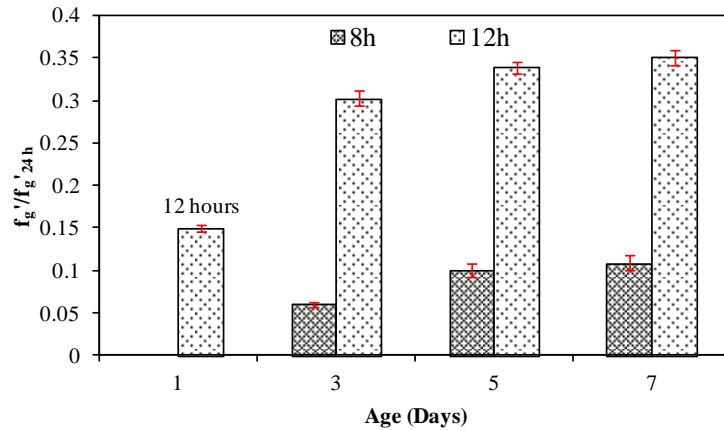


Figure 4.4: Ratio of compressive strength for varying initial curing periods to the 7-day strength of specimens initially cured for 1 day.

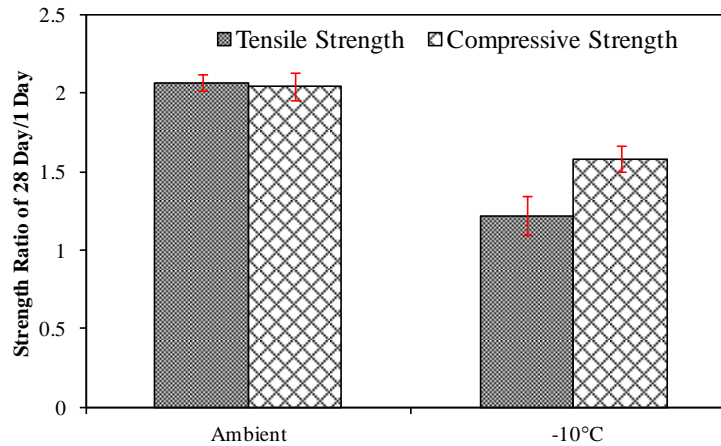
4.4.2 Tensile Strength

The results of tensile strength, $f_{g,t}$, young's modulus, E_g , and poisson's ratio, ν_g , of grout specimens cured under various temperature regimes are displayed in **Table 4.2**. It can be observed that there was steady increase in tensile strength up to 28 days for specimens cured at ambient temperature. However, specimens cured at -10°C achieved limited tensile strength gain after 1 day of ambient temperature curing.

The ratio of the 28-day to the 1-day tensile and compressive strengths for specimens cured at ambient and -10°C curing is displayed in **Fig. 4.5**. It can be observed that the subfreezing curing was more detrimental to the tensile strength than to the compressive strength. Specimens cured at ambient temperatures experienced a gain of 105% in compressive strength, and 107% in tensile strength, between 1 and 28 days, respectively. Yet, specimens cured at -10°C experienced a gain of only 59% in compressive strength and 22% in tensile strength between 1 and 28 days, respectively. This contradicts the results of previous studies that concluded that exposure of concrete to subfreezing resulted in lower percentage of compressive strength gain than that of tensile strength gain (Marzouk & Hussein, 1995).

Table 4.2: Grout tensile strength, Young's modulus, and Poisson's ratio

Temperature	Age (Days)	$f_{g,t}$ (MPa)	E_g (MPa)	ν_g
Ambient (23°C)	1	3.02	-	-
	3	3.29	-	-
	7	4.49	20712	0.2285
	28	6.25	22713	0.2346
-10°C	1	3.01	-	-
	3	3.18	-	-
	7	3.22	19971	0.2315
	28	3.68	20563	0.2322

**Figure 4.5:** Ratio of 28-day to the 1-day tensile and compressive strengths for varying curing temperatures.

4.4.3 Modulus of Elasticity

It can be observed in **Table 4.2** that the modulus of elasticity of the grout was adversely affected by subfreezing exposure. For instance, specimens initially cured at ambient temperature for one day then exposed to -10°C achieved 96% of the modulus of elasticity of the control specimens cured at ambient conditions at 7 days, and 90% at 28 days. The increase in modulus of elasticity is greatly slowed between 7 and 28 days for specimens cured at -10°C, with a minimal gain of 3%. Yet, the control specimens cured at ambient temperature achieved 10% gain in modulus between 7 and 28 days. A similar trend was observed by Marzouk & Hussein (1995), who found that the modulus of elasticity

increased by 5% from 7 to 28 days, despite subfreezing exposure, yet at a much slower rate compared to that at ambient curing.

4.4.4 Thermogravimetric Analysis

Differential thermogravimetric analysis (DTG) and thermogravimetric analysis (TGA) curves for grout specimens exposed to various temperature curing regimes are presented in **Figs. 4.6** and **4.7**, respectively. It can be observed in **Fig. 4.6** that there are three major peaks for all tested specimens with slight change in intensity or temperature range. These peaks represent the decomposition of different compounds in the hydrated grout matrix as displayed in **Fig. 4.7**. The first peak between 25 and 200°C corresponds to the dehydration of CSH and ettringite. The removal of free water is also typically observed in this temperature range. However, the desiccation performed during the specimen preparation is assumed to have removed free water. The main peak is attributed to the decomposition of calcium silicate hydrate (CSH) gel, while the shoulder to the right of the peak at around 140°C is associated with ettringite (Sha, O'Neill, & Guo, 1999; Soriano et al., 2013). The second zone between 375 and 480°C is attributed to the de-hydroxylation of calcium hydroxide, also known as portlandite (Trník et al., 2016). The third zone between 525 and 750°C is attributed to the de-carbonation of calcium carbonate. There are two forms of calcium carbonate present: a poorly crystallized vaterite, which is an unstable form of calcium carbonate (Cole & Kroone, 1960; Šauman, 1971); and the more stable calcite, which decomposes at a higher temperature than vaterite (Trník et al., 2016). This can be observed by examining the DTG curve in **Fig. 4.6** for the specimen cured for 7-days at ambient temperature, where two smaller sub-peaks were present in the 525 to 750°C range.

Since the decomposition of CSH and ettringite overlap, it is difficult to accurately quantify the contents of either of these components. However, the portlandite and calcium carbonate contents can be estimated from the TGA results using the measured mass change and the decomposition reactions (**Eq. 4.1** and **Eq. 4.2**) with their theoretical mass losses (Dweck, Buchler, Coelho, & Cartledge, 2000; Trník et al., 2016):

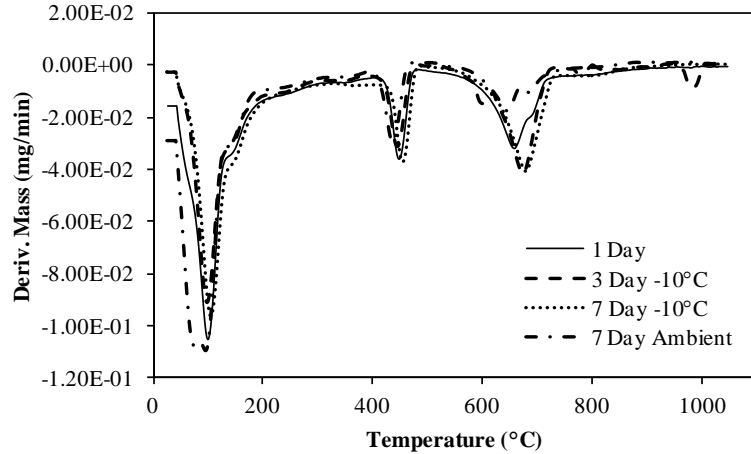
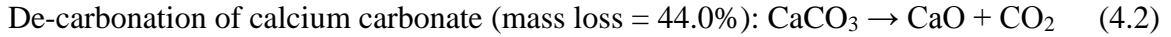
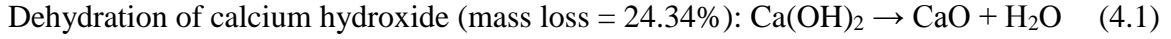


Figure 4.6: DTG curves for grout specimens at different ages and curing conditions.

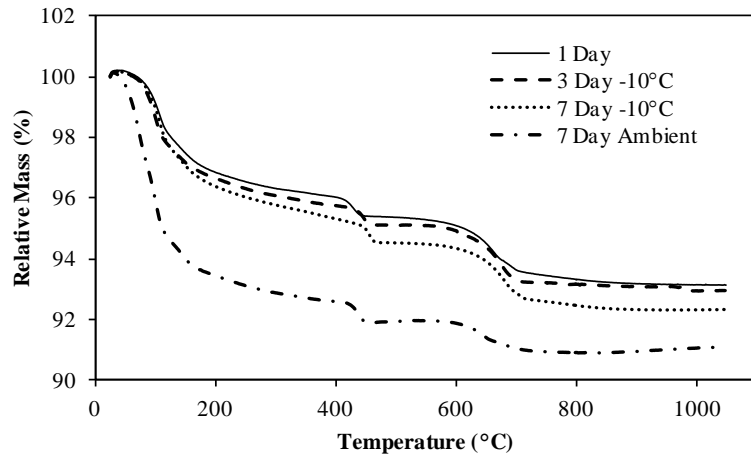


Figure 4.7: TGA curves for grout specimens at different ages and curing conditions.

From the TGA results in **Table 4.3**, it can be observed that there was notable increase in portlandite between 1 and 7 days for grout specimens cured 1 day at ambient temperature and then at -10°C up to 7 days. This is apparently due to the progress of hydration reactions under subfreezing conditions, since the amount of CSH/ettringite also continued to grow, accompanied by increased mechanical properties. However, the control

specimen cured for 7 days at ambient temperature had a much smaller increase in portlandite, and a much larger increase in CSH/ettringite. Hence, it appears that this relatively large increase in portlandite under subfreezing conditions is indicative of the pozzolanic reactions of fly ash incorporated in the grout being significantly hampered compared to the main cement hydration process under subfreezing temperatures, as previously hypothesized by other researchers (Marzouk & Hussein, 1995). This is also supported by previous researchers who have shown that the portlandite content decreased with hydration time for concretes incorporating pozzolans (Payá, Monzó, Borrachero, & Velázquez, 2003; Pinto et al., 2007; Soriano et al., 2013; Trník et al., 2016; Vedalakshmi et al., 2003).

Table 4.3: Relative mass change (in %) and calculated content (in %) of the corresponding hydration products

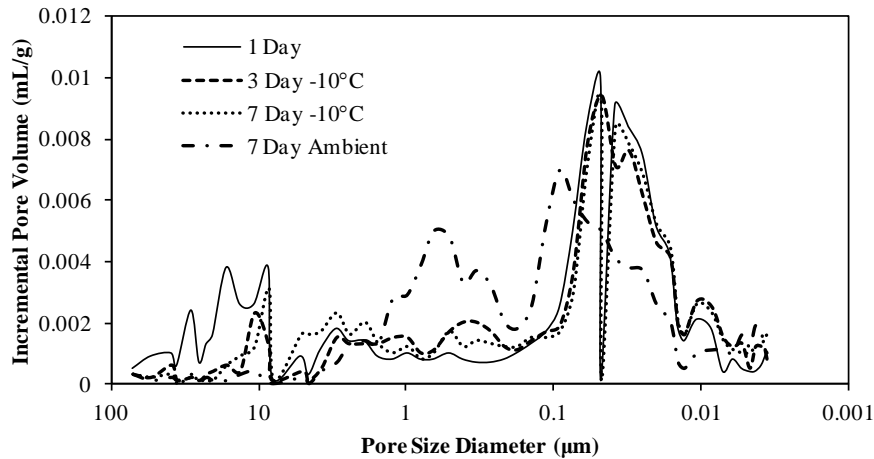
Temperature	Age (Days)	CSH and Ettringite	Portlandite		Calcium Carbonate	
		Mass Change	Mass Change	Content	Mass Change	Content
Ambient (23°C)	1	-3.19	-0.71	2.90	-1.88	4.28
	7	-6.55	-0.74	3.06	-1.03	2.33
-10°C	3	-3.37	-0.70	2.89	-1.91	4.33
	7	-3.63	-0.90	3.70	-1.91	4.35

4.4.5 Mercury Intrusion Porosimetry

Table 4.4 and **Fig. 4.8** exhibit the MIP test results for grout specimens at various ages subjected to different curing conditions. The results show that the total intrusion volume and average pore diameter decreased from 1 day to 7 days for both specimens cured at ambient temperature and at -10°C. The specimens cured at -10°C had greater total intrusion volume compared to that of specimens cured at ambient temperature, indicating higher total porosity, likely due to less advanced cement hydration reactions. A greater decrease in average pore diameter was observed in the subfreezing curing condition (0.0266 μm) compared to that at ambient temperature curing (0.0321 μm). While it has been known that curing cement based materials at lower temperature normally leads to more refined microstructure and smaller pore size, it is not sure whether the effect observed herein is an artifact or a real phenomenon.

Table 4.4: Average pore size and total intrusion volume from MIP test

Temperature	Age (Days)	Average Pore Diameter (μm)	Total Intrusion Volume (mL/g)
Ambient (23°C)	1	0.0369	0.113
	7	0.0321	0.1003
-10°C	3	0.0293	0.1091
	7	0.0266	0.1052

**Figure 4.8:** Incremental pore intrusion volume versus pore diameter for grout specimens at different ages and curing conditions.

Comparing the incremental pore intrusion volume versus pore diameter for grout specimens cured at ambient conditions for 1 and 7 days (**Fig. 4.8**), it can be observed that the specimens cured for 7-days at ambient temperature had a decrease in the larger pore sizes ($>1\mu\text{m}$), as well as a decrease in the smaller pore sizes ($<0.07\mu\text{m}$) compared to the specimens cured similarly for only one day. The majority of pores ranged from 1 to $0.02\mu\text{m}$ in diameter. The peak was also much smaller for the 7-day specimens, resulting in lower total intrusion volume as expected. For both specimens cured for 3 and 7 days at -10°C , there was a minimal pore refinement effect taking place. Aside from a decrease in pore sizes larger than $10\mu\text{m}$, the pore size distribution has changed negligibly. This further supports the argument that pozzolanic reactions are significantly slowed or halted at subfreezing temperatures.

4.4.6 Bond Behaviour of Grouted Dowel

Test results of 10 pullout specimens are summarized in **Table 4.5**. The specimen notation is as follows (*lT-n*), where *l* indicates the embedment length (*l* = 6, 12, or 16 bar diameters), T represents the curing temperature (*T* = A for ambient, or 10 for -10°C), and *n* represents the specimen number. Specimens cured at -10°C, were initially maintained at ambient for one day. The yielding displacement, δ_y (mm), is taken as the point on the bar stress-displacement plot where the specimen's stiffness degraded suddenly after the elastic response. The ultimate displacement, δ_u (mm), and maximum slip, s_{max} (mm), correspond to the point where the maximum load, P (kN), occurs. The maximum bond stress, u_b (MPa), is calculated assuming an average stress distribution along the bar (**Eq. 4.3**).

$$u_b = \frac{P \times 10^3}{\pi \cdot d_b \cdot l_d} \quad (4.3)$$

Table 4.5: Pullout test results

Specimen	P (kN)	f_s (MPa)	δ_y (mm)	δ_u (mm)	s_{max} (mm)	u_b (MPa)	R_s	μ_d	Failure Mode
6-A-1	250.8	510.9	16.3	54.8	0.96	21.0	1.28	3.4	Pullout
6-A-2	243.6	496.3	13.5	43.8	1.02	20.4	1.24	3.2	Pullout
6-10-1	235.9	480.6	16.2	22.4	0.93	19.7	1.20	1.4	Pullout
6-10-2	217.6	443.3	14.0	21.7	0.60	18.2	1.11	1.6	Pullout
12-A-1	273.1	556.4	12.4	110.4	0.09	11.4	1.39	8.9	Fracture
12-A-2	273.4	557.0	12.7	104.0	0.05*	11.4	1.39	8.2	Fracture
12-10-1	277.6	565.5	11.3	86.5	0.82	11.6	1.41	7.6	Pullout
12-10-2	271.1	552.3	12.1	72.8	0.97	11.3	1.38	6.0	Pullout
16-10-1	293.1	597.1	13.2	113.6	0.05*	9.2	1.49	8.6	Fracture
16-10-2	290.7	592.2	12.5	100.5	0.11	9.1	1.48	8.1	Fracture

Note: * LVDT measuring slip malfunctioned before peak slip was reached.

The bar stress-displacement behavior of each specimen type is displayed in **Fig. 4.9**. The recorded displacement is the relative movement of the testing machine's crossheads; this therefore accounts for both slip and bar elongation. For all specimens, the behavior mimicked that of a regular steel bar until the peak load was reached. For specimens experiencing a pullout failure, a steep drop in load then occurred until a small plateau was reached due to the residual bond stress, then the test was stopped.

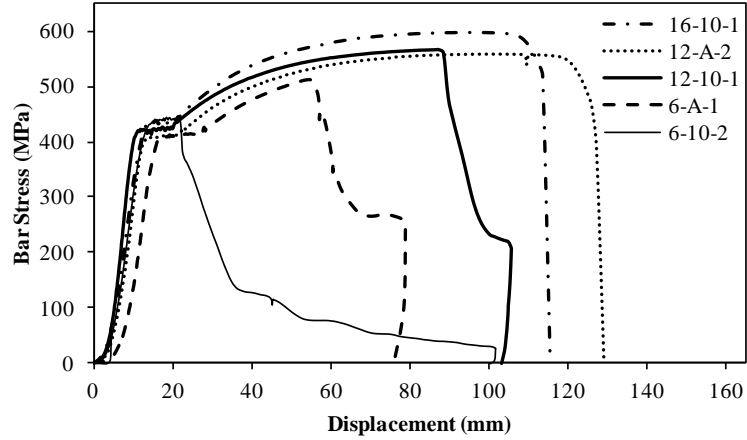


Figure 4.9: Bar stress-displacement plots for each embedment length and curing regime.

As previously discussed in Chapter 3, mechanical splices, which are also commonly used as precast concrete wall panel connections, are required by current design codes to develop 125% of the bars yield strength to account for material over-strength and ensure that the bar yields (ACI Committee 318, 2014). Therefore, the same strength ratio, R_s , (Eq. 3.2) was used herein.

It has been established that precast concrete connections in low to moderate seismic regions require a ductility ratio of 4.0 (Soudki, Rizkalla, & Leblanc, 1995). This ratio was therefore used herein since there are minimal code requirements for proving the adequacy of these connections. The ductility ratio, μ_{Δ} , is the ratio between the ultimate displacement and the yielding displacement (Eq. 4.4).

$$\mu_{\Delta} = \frac{\delta_u}{\delta_y} \quad (4.4)$$

Specimens with an embedment length of 6 bar diameters cured at ambient temperature achieved the required strength ratio; however they did not achieve the minimum ductility requirements. All specimens with an embedment length of 12 bar diameters or longer achieved both a strength ratio greater than 1.25 and a ductility ratio greater than 4.0, regardless of the curing conditions. This demonstrates that an embedment length of 12 bar diameters or longer is sufficient in this connection using the grout investigated herein, even when early-age subfreezing exposure occurs.

4.4.6.1 Failure Modes

There were only two failure modes exhibited by all pullout specimens, pullout failure consisting of bar-grout bond failure (**Fig. 4.10a**), and bar fracture (**Fig. 4.10b**). In practical applications, bar fracture is the preferred failure mode since it allows the bar to fully develop, therefore offering higher tensile capacity for the connection. It also provides desired superior ductility through the bar post-yielding elongation. No cracking of the concrete block was observed for all tested specimens. Also, since the bars were wrapped, no conical failure of the grout at the active end was experienced, as observed in Chapter 3, and reported by previous researchers investigating similar connections (Steuck et al., 2009).

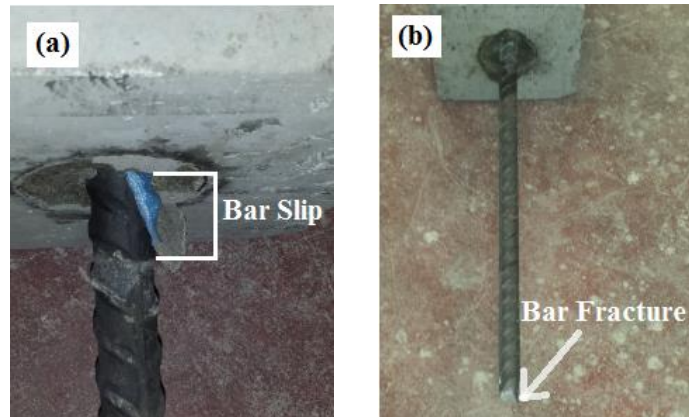


Figure 4.10: Failure modes of pullout specimens: (a) bar pullout; (b) bar fracture.

4.4.6.2 Bond Strength

Specimens 12-10-1 and 12-10-2 (both having embedment length of 12 bar diameter) experienced pullout failure at a much lower bond stress than that of specimens with embedment lengths of 6 bar diameters. This can be attributed to the fact that these specimens reached very close to their fracture loads, and have therefore undergone significant yielding. This can be observed in **Fig. 4.9**, where specimen 12-10-1 achieved nearly 83% of the yielding of specimen 16-10-1. Yielding results in inelastic elongation that reduces the diameter of the bar, partially disengaging it from the surrounding grout, and can therefore reduce the bond strength.

At first, the bond strength appeared to be noticeably affected by the -10°C curing temperature for specimens with embedment lengths of 6 bar diameters. However, previous research has reported that the average bond stress is directly proportional to the square root of the concrete compressive strength (Untrauer & Henry, 1965), even under low temperature curing (Gardner & Poon, 1976). Therefore, to accurately analyze the effect of subfreezing exposure on bond strength, the peak bond strength, u_b , was normalized with the square root of the grout compressive strength, $\sqrt{f'_g}$. The normalized bond strength was plotted versus the corresponding normalized length for all specimens as displayed in **Fig. 4.11**.

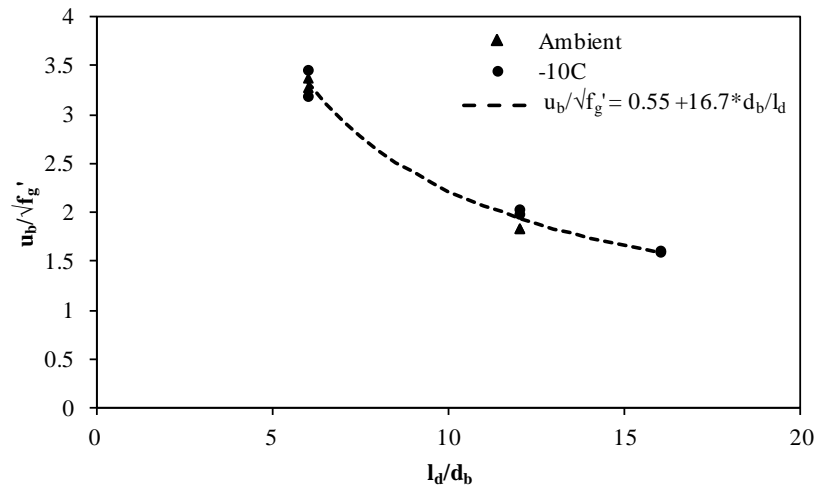


Figure 4.11: Normalized bond stress versus normalized embedment length.

It can be observed in **Fig. 4.11** that there is very little difference in the normalized bond strength between specimens cured at ambient temperature or at -10°C . Indeed, the reduction in average bond strength for specimens having an embedment length of 6 bar diameters cured at ambient temperature versus -10°C was 8.3%, and the reduction in the square root of compressive strength was 8.1%. This indicates that the bond strength remained directly proportional to the square root of the compressive strength of the grout as previously established, regardless of the early age exposure of specimens to subfreezing. The peak bond strength, u_b , normalized with the square root of the grout compressive strength, $\sqrt{f'_g}$, for the various curing conditions was fit using **Eq. 4.5** below, with a coefficient of correlation of 0.987 as shown in **Fig. 4.11**.

$$\frac{u_b}{\sqrt{f'_g}} = 0.55 + 16.7 * d_b / l_d \quad (4.5)$$

Where,

$\frac{u_b}{\sqrt{f'_g}}$ = normalized bond strength ($\sqrt{\text{MPa}}$);

d_b = bar diameter (mm);

l_d = development length (mm).

This fit followed a similar behaviour to the relationship proposed by Orangun et al. (1977), which provides the basis for the current ACI 318-14 equation (25.4.2.3). However, this trend does not adequately represent the behavior of specimens in the elastic range when compared to results from Chapter 3 and previous research (Steuck et al., 2009), and is therefore only applicable for specimens that have undergone extensive yielding. For practical purposes, it is desirable to know how the bar stress and required development length are affected by the change in compressive strength due to exposure to subfreezing temperature. Since the change in bond strength is directly proportional to the change in the square root of the grout's compressive strength, and knowing that through equilibrium,

$$u_b = \frac{f_s d_b}{4l_d} \quad (4.6)$$

It can be concluded that the bar stress will also be affected proportionally, and the required development length is inversely proportional to the change in the square root of the grout's compressive strength. Therefore, the development length will require an increase by the same magnitude that the square root of grout compressive strength is decreased. For example, a decrease in compressive strength from 40 MPa to 30 MPa due to early-age subfreezing exposure would require a development length 1.13 times longer.

4.4.6.3 Bond Stress-Slip Response

All pullout test specimens with an embedment length of 6 bar diameters had a similar bond stress-slip response. Specimens 12-10-1 and 12-10-2, which have embedment length of 12 bar diameter, behaved differently due to the much lower peak bond stress reached. However, they have similar characteristic regions to that of the pullout specimens with embedment length of 6 bar diameters, but smaller in scale due to their lower peak bond stresses. The bond stress-slip response of specimens 6-A-2, 6-10-1, and 12-10-2 are shown in **Fig. 4.12**, along with previously established models for the grouted dowel connection.

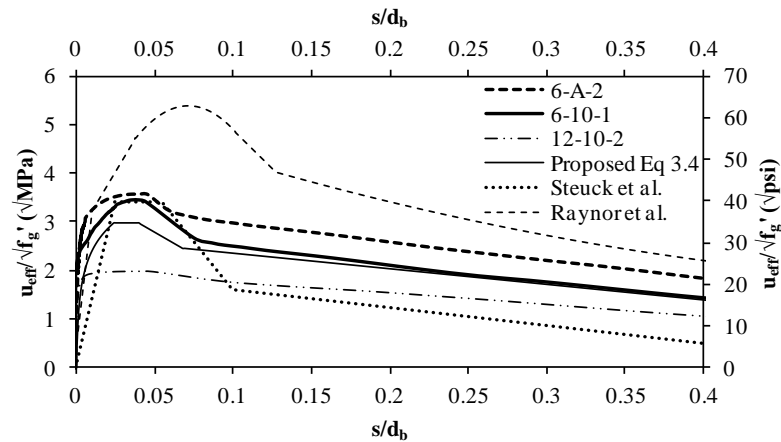


Figure 4.12: Bond stress-slip response for each embedment length and curing regime compared to established models.

The bond stress-slip response of all pullout specimens is characterized by four regions: i) a curvilinear ascending branch from the beginning of the test until the peak bond stress was reached; ii) a region of approximately constant stress at the peak bond stress; iii) an approximately linear region of sudden decrease until the residual bond stress; and iv) a linear region with a more gradual decrease in bond stress until the test was stopped. Specimens with a longer embedment length (12 bar diameters) had a much stiffer ascending branch than that of specimens with an embedment length of 6 bar diameters, experiencing minimal slip until the peak bond stress was reached. This may be due to the extensive yielding undergone by specimens 12-10-1 and 12-10-2, leading to significant

reduction in the bar-cross section, which disengaged the bar from the grout, causing sudden failure and resulting in little slip beforehand.

It can be observed in **Fig. 4.12** that the specimens having an embedment length of 6 bar diameters followed similar behavior to the model previously developed in Chapter 3, except with larger peak bond stresses. Such peak bond stresses are comparable to that predicted by the Steuck et al. (2009) model, and are likely due to differences in test setup. It can be observed that the only difference in bond-slip behavior between specimens cured at ambient and -10°C is the third region where the bond stress suddenly decreased to the residual bond stress. However, it is difficult to determine whether this is substantial since such small differences have been reportedly due to the variable nature of concrete (Eligehausen et al., 1983).

4.5 Summary and Conclusions

The objective of this study was to investigate the effects of early-age exposure to subfreezing temperature on the performance of grouted dowel connections commonly used in precast concrete wall panel construction. The mechanical properties, pore size distribution, and progress of hydration reactions in the grout were examined as a function of the curing regime. Based on the experimental results, the following conclusions can be drawn:

1. Lower curing temperature resulted in lower compressive strength of the grout, as expected. However, there was no significant difference in compressive strength for grouts cured at -10°C and -20°C .
2. The initial curing time at ambient temperature ($23 \pm 1^{\circ}\text{C}$) was crucial for the grout's compressive strength development. Reducing this initial curing time of 24 hours by half to 12 hours reduced the compressive strength by 65%.
3. Curing the grout at -10°C was more detrimental to the tensile strength gain than to the compressive strength gain. When cured at -10°C , the increase in strength gain between 1 and 28 days was 59% for compressive strength, yet only 22% for tensile strength.

4. The development of the modulus of elasticity was greatly slowed between 7 and 28 days subsequent to early-age exposure of the grout to subfreezing conditions.
5. Pozzolanic reactions appeared to be greatly slowed or halted compared to the basic cement hydration reactions when the grout was cured at early-age under subfreezing conditions.
6. Curing the grout at -10°C resulted in greater total mercury intrusion volume compared to that for specimens cured at ambient temperatures, indicating higher total porosity.
7. The bond strength of the grouted dowel connection remained proportional to the square root of the grout compressive strength even after early-age subfreezing exposure. Furthermore, curing the grout at -10°C resulted in an increase in the dowel embedment length from 12 to 16 bar diameters to achieve bar fracture.
8. The bond stress-slip response of the grouted dowel connection remained unchanged for specimens exposed to early-age subfreezing conditions.
9. The mechanical properties and their associated strength development under subfreezing conditions found herein are only applicable to the specific grout tested. As discussed in Chapter 2, different cementitious proportions will result in different final strengths, and rate of strength gain under subfreezing conditions. Therefore, it is important to accurately test the desired grout for use in subfreezing conditions.

4.6 References

- ACI Committee 306. (2010). Guide to Cold Weather Concreting (ACI 306R-10). *American Concrete Institute*. Farmington Hills, MI, USA.
- ACI Committee 318. (2014). Building Code Requirements for Structural Concrete (ACI 318-14) and Commentary (ACI 318R-14). *American Concrete Institute*. Farmington Hills, MI.
- ACI Committee 408. (2003). Bond and Development of Straight Reinforcing Bars in Tension (ACI 408-03). *American Concrete Institute*. Farmington Hills, MI, USA.

- Aitcin, P.-C., Cheung, M. S., & Shah, V. K. (1985). Strength Development of Concrete Cured Under Arctic Sea Conditions. *Temperature Effects on Concrete*. ASTM International.
- ASTM C39. (2016). Standard Test Method for Compressive Strength of Cylindrical Concrete Specimens. *American Society for Testing and Materials*. West Conshohocken, PA. doi:10.1520/C0039
- ASTM C469. (2014). Standard Test Method for Static Modulus of Elasticity and Poisson's Ratio of Concrete in Compression. *American Society for Testing and Materials*. West Conshohocken, PA. doi:10.1520/C0469
- ASTM C496. (2011). Standard Test Method for Splitting Tensile Strength of Cylindrical Concrete Specimens. *American Society for Testing and Materials*. West Conshohocken, PA. doi:10.1520/C0496
- Bhatty, J. (1991). A review of the application of thermal analysis to cement-admixture systems. *Thermochimica Acta*, 189, 313–350. doi:10.1016/0040-6031(91)87128-J
- Cole, W. F., & Kroone, B. (1960). Carbon Dioxide in Hydrated Portland Cement. *Journal of the American Concrete Institute*, 56(6), 1275–1296.
- Dweck, J., Buchler, P. M., Coelho, A. C. V., & Cartledge, F. K. (2000). Hydration of a Portland cement blended with calcium carbonate. *Thermochimica Acta*, 346(1-2), 105–113. doi:10.1016/S0040-6031(99)00369-X
- Eligehausen, R., Popov, E. P., & Bertero, V. V. (1983). Local bond stress-slip relationships of deformed bars under generalized excitations. *Report No. UCB/EERC-83/23*. Earthquake Engineering Research Center, University of California-Berkeley.
- Gardner, N. J. (1990). Effect of Temperature on the Early-Age Properties of Type I, Type III, and Type I/ Fly Ash Concretes. *ACI Materials Journal*, 87(1), 68–78.
- Gardner, N. J., & Poon, S. M. (1976). Time and Temperature Effects on Tensile, Bond, and Compressive Strengths. *ACI Journal Proceedings*, 73(7), 405–409.
- Gardner, N. J., Sau, P. L., & Cheung, M. S. (1988). Strength development and durability of concretes cast and cured at 0 C. *ACI Materials Journal*, 85(6), 529–536. doi:10.14359/2289
- Husem, M., & Gozutok, S. (2005). The effects of low temperature curing on the compressive strength of ordinary and high performance concrete. *Construction and Building Materials*, 19(1), 49–53. doi:10.1016/j.conbuildmat.2004.04.033
- Klieger, P. (1958). Effect of mixing and curing temperature on concrete strength. *ACI Journal*, 54(6), 1063–1081.
- Marzouk, H., & Houssein, A. (1990). Properties of high-strength concrete at low temperatures. *ACI Materials Journal*, 87(2), 167–171.
- Marzouk, H., & Hussein, A. (1995). Effect of Curing Age on High-Strength Concrete at Low Temperatures. *Journal of Materials in Civil Engineering*, 7(3), 161–167. doi:10.1061/(ASCE)0899-1561(1995)7:3(161)

- Nassif, A. Y., & Petrou, M. F. (2013). Influence of cold weather during casting and curing on the stiffness and strength of concrete. *Construction and Building Materials*, *44*, 161–167. doi:http://dx.doi.org/10.1016/j.conbuildmat.2013.03.016
- Orangun, C.O., Jirsa, J. O., & Breen, J. E. (1977). A reevaluation of test data on development length splices. *Journal of the American Concrete Institute*, *74*(3), 114-122. doi:10.14359/10993
- Payá, J., Monzó, J., Borrachero, M., & Velázquez, S. (2003). Evaluation of the pozzolanic activity of fluid catalytic cracking catalyst residue (FC3R). Thermogravimetric analysis studies on FC3R-Portland cement pastes. *Cement and Concrete Research*, *33*(4), 603–609. doi:10.1016/S0008-8846(03)00014-0
- Pinto, C. A., Büchler, P. M., & Dweck, J. (2007). Pozzolanic properties of a residual FCC catalyst during the early stages of cement hydration: Evaluation by thermal analysis. *Journal of Thermal Analysis and Calorimetry*, *87*(3), 715–720. doi:10.1007/s10973-006-7772-2
- Raynor, D. J., Dawn, E. L., & Stanton, J. F. (2002). Bond-Slip Response of Reinforcing Bars Grouted in Ducts. *ACI Structural Journal*, *99*(5), 568–576.
- Šauman, Z. (1971). Carbonization of porous concrete and its main binding components. *Cement and Concrete Research*, *1*(6), 645–662.
- Sha, W., O'Neill, E. a., & Guo, Z. (1999). Differential scanning calorimetry study of ordinary Portland cement. *Cement and Concrete Research*, *29*(9), 1487–1489. doi:10.1016/S0008-8846(99)00128-3
- Shih, T. S., Lee, G. C., & Chang, K. C. (1988). Effect of Freezing Cycles on Bond Strength of Concrete. *Journal of Structural Engineering*, *114*(3), 717–726. doi:10.1061/(ASCE)0733-9445(1988)114:3(717)
- Soriano, L., Monzó, J., Bonilla, M., Tashima, M. M., Payá, J., & Borrachero, M. V. (2013). Effect of pozzolans on the hydration process of Portland cement cured at low temperatures. *Cement and Concrete Composites*, *42*, 41–48. doi:10.1016/j.cemconcomp.2013.05.007
- Soudki, K. A., Rizkalla, S. H., & Leblanc, B. (1995). Horizontal Connections for Precast Concrete Shear Walls Subjected to Cyclic Deformations Part 1: Mild Steel Connections. *PCI Journal*, *40*(4), 78–96.
- Steuck, K. P., Eberhard, M. O., & Stanton, J. F. (2009). Anchorage of large-diameter reinforcing bars in ducts. *ACI Structural Journal*, *106*(4), 506–513.
- Trník, A., Scheinherrová, L., Kulovaná, T., & Černý, R. (2016). Simultaneous Differential Scanning Calorimetry and Thermogravimetric Analysis of Portland Cement as a Function of Age. *International Journal of Thermophysics*, *37*(1), 12. doi:10.1007/s10765-015-2028-7
- Untrauer, R. E., & Henry, R. L. (1965). Influence of Normal Pressure on Bond Strength. *ACI Journal*, *62*(5), 577–586.
- Vedalakshmi, R., Raj, A. S., Srinivasan, S., & Babu, K. G. (2003). Quantification of hydrated cement products of blended cements in low and medium strength

concrete using TG and DTA technique. *Thermochimica Acta*, 407(1-2), 49–60.
doi:10.1016/S0040-6031(03)00286-7

5 SUMMARY AND CONCLUSIONS

5.1 Summary

Precast concrete load-bearing wall panels have become a popular choice for low-, medium-, and high-rise construction in North America. An integral part of this structural system is the horizontal connections between wall panels, since it directly affects the strength and stability of the structure. A very common connection method is the grouted dowel connection, where a reinforcing bar protruding from the lower wall panel is grouted into a corrugated steel duct cast into the upper wall panel. Despite the common use of this connection in practice, there are no pertinent specific code requirements that guide this use, and related research is sparse. Furthermore, this construction proceeds throughout cold weather conditions, with the connection area typically heated for one day then exposed to subfreezing temperatures, before the grout is fully cured. The effects of exposure to early-age subfreezing temperatures on the bond behaviour of this connection are still not well understood. Thus, the focus of this research was to fill this knowledge gap by exploring the bond behaviour of this connection for use in precast wall panel construction, and the effects of exposure to early-age subfreezing temperatures on the connection's bond strength.

Chapter 2 presented a literature review of the mechanisms of bond, as well as the few relevant studies that have examined this connection. It was shown that this connection is currently designed as a regular reinforcing bar in concrete (ACI Committee 318, 2014), which does not account for the additional confinement provided by the presence of the corrugated steel duct. It was also demonstrated that when greater confinement is present, it can lead to greatly oversized embedment lengths (Einea et al., 1999). The only available study on the bond strength of this connection examined its use for precast bridge bent caps using larger diameter bars (32M to 57M), with larger duct diameter/bar diameter ratios of 3.6 (Steuck et al., 2009), whereas a typical wall panel connection generally uses a 25M bar with a duct diameter/bar diameter ratio of 3.0. This demonstrates the lack of information available on this connection, specifically for its use in precast wall panels. Furthermore, there is a lack of research in the open literature examining the effects of subfreezing curing on bond strength. Yet, one study

investigating the effect of 2°C curing on concrete concluded that the bond strength remained proportional to the square root of compressive strength, irrespective of the temperature or cement type (Gardner & Poon, 1976). It was concluded from this literature review that the corrugated steel duct present in this connection generates greater confinement than what is accounted for in the current design codes, allowing for a reduction in development length compared to a regular bar in traditional reinforced concrete. Yet, the limited research available requires further investigation into this connection for its use in precast wall panels, along with thorough examination of how the exposure to early-age subfreezing temperatures affects the bond strength of the connection.

Chapter 3 comprised an experimental investigation on the grouted dowel connection specific to precast wall panel construction. The experimental program consisted of eighteen pullout test specimens to determine the bond strength of the connection. Moreover, the effect of the duct and eccentricity of bar placement within the duct were examined. The results of this investigation were analyzed and compared to existing data from Steuck et al. (2009). From these results, a design equation was developed to predict the development length of this connection, which accounts for the effect of bar size, steel strength, and grout compressive strength. The results were also compared to the current ACI 318-14 equation (25.4.2.3), and the equation developed by Steuck et al. (2009). A bond stress-slip model was also proposed and compared to established models.

Chapter 4 investigated the effects of exposure to early-age subfreezing temperature on the mechanical properties of the grout and the bond strength of the connection. For this purpose, specimens were initially cured for one day at ambient temperature and then placed inside a walk-in environmental chamber at -10°C. The hardened grout properties were analyzed and compared to specimens cured at ambient temperature. The compressive strength of the grout was monitored at additional temperatures of 1°C and -20°C. The effects of subfreezing curing on the grout's hydration products development was also examined through the use of thermogravimetric analysis. Furthermore, mercury intrusion porosimetry tests were performed to examine how the subfreezing curing affected the porosity and pore size distribution of the grout. The effects of early-age

exposure to subfreezing temperature on the bond strength of the connection were quantified, and recommendations for cold weather construction were provided.

5.2 Conclusions

The major conclusions of this research are as follows:

1. The steel duct creates a higher confinement effect than present in regular reinforced concrete, allowing for a shear pullout failure rather than a tensile splitting failure. This failure mode occurs at significantly higher bond stresses, allowing for a reduction in required embedment length. The absence of the corrugated steel duct results in a tensile splitting failure, and can reduce the strength of this connection by about 30%.
2. Eccentric bar placement generates tensile stress concentrations in the surrounding concrete, which can result in tensile splitting of the concrete not observed in specimens with concentric bar placement. This results in about 10% strength reduction for embedment lengths of 12 bar diameters, and 4% for embedment lengths of 36 bar diameters.
3. The current ACI 318-14 equation (25.4.2.3) does not account for the greater confinement effect of the duct. It therefore greatly overestimates the required development length, resulting in values 3.08 times larger than required.
4. The equation proposed by Steuck et al. (2009) is not sufficiently conservative, which is a disadvantage for designing the grouted dowel connection since safety is necessary considering the high variability of concrete materials. The equation proposed in the present study is 10% on the conservative side, which is a desirable feature in design applications.
5. The equation proposed in the present study is applicable for non-shrink grouts having a compressive strength up to 70 MPa. Using other grout types has not been investigated herein, and thus needs to be validated for specific use in this particular connection. The use of higher strength grouts (>70 MPa) has also not been explored, and therefore the proposed design equation should be limited to 70 MPa until such data on using higher strength grouts becomes available.

6. Lower curing temperature resulted in lower compressive strength of the grout, as expected. However, there was no significant difference in compressive strength for grouts cured at -10°C and -20°C . The initial curing time at ambient temperature ($23 \pm 1^{\circ}\text{C}$) was crucial for the grout's compressive strength development. Reducing this initial curing time by half reduced the compressive strength by 65%.
7. Curing the grout at -10°C was more detrimental to the tensile strength gain than to the compressive strength gain. When cured at -10°C , the increase in strength gain between 1 and 28 days was 59% for compressive strength, yet only 22% for tensile strength.
8. The development of the modulus of elasticity was greatly slowed between 7 and 28 days subsequent to the early-age exposure of the grout to subfreezing conditions.
9. Pozzolanic reactions appeared to be greatly slowed/halted compared to the basic cement hydration reactions when the grout was exposed to early-age subfreezing temperatures.
10. Curing the grout at -10°C resulted in greater total mercury intrusion volume compared to that for specimens cured at ambient temperatures, indicating higher total porosity.
11. The bond strength of the grouted dowel connection remained proportional to the square root of the grout compressive strength even after early-age subfreezing exposure. Furthermore, curing the grout at -10°C resulted in an increase in the embedment length from 12 to 16 bar diameters to achieve bar fracture.
12. The bond stress-slip response of the grouted dowel connection remained unchanged for specimens exposed to early-age subfreezing conditions.
13. The mechanical properties and their associated strength development under subfreezing conditions found herein are only applicable to the specific grout tested. As discussed in Chapter Two, different cementitious proportions will result in different final strengths, and rate of strength gain under subfreezing conditions. Therefore, it is important to accurately test the desired grout for use in subfreezing conditions.

5.3 Recommendations for Future Work

Recommendations for future work are as follows:

1. A relationship between monotonic and cyclic loading is yet to be established for grouted dowel connections. Therefore, the connection behaviour under seismic loading should be examined, specifically, with special focus on possible increase in development length required for use in seismic applications.
2. Determine the behaviour of the entire non-contact lap splice. The present research examined the required development length of the grouted dowel alone. Therefore, it is unknown if this reduction in length is sufficient to lap the existing reinforcement in the wall panel.
3. Full-scale wall panel testing under flexural loading should also be examined to determine the effect of combined shear and tension stresses.
4. The use of high strength grout (>70 MPa) should be explored for use in this connection. Currently the design equation is limited to a compressive strength of 70 MPa due to the lack of data available.
5. The mechanisms of cement hydration at subfreezing conditions are yet to be clearly established. This research has shown that the cement hydration reactions continued when the internal temperature was as low as -20°C , well below the freezing point of water. Other researchers have hypothesized reasons for the freezing point of water to be depressed and/or delayed. Yet, no relevant and substantial evidence has been yet produced. This issue needs dedicated research effort.

5.4 References

- ACI Committee 318. (2014). Building Code Requirements for Structural Concrete (ACI 318-14) and Commentary (ACI 318R-14). *American Concrete Institute*. Farmington Hills, MI.
- Einea, A., Yehia, S., & Tadros, M. K. (1999). Lap splices in confined concrete. *ACI Structural Journal*, 96(6), 947–955.
- Gardner, N. J., & Poon, S. M. (1976). Time and Temperature Effects on Tensile Bond, and Compressive Strengths. *ACI Journal Proceedings*, 73(7), 405–409.

Steuck, K. P., Eberhard, M. O., & Stanton, J. F. (2009). Anchorage of large-diameter reinforcing bars in ducts. *ACI Structural Journal*, 106(4), 506–513.

APPENDICES

Table A.1: Compressive strength data of grout cured at ambient ($23 \pm 1^\circ\text{C}$)

Age (Days)	Sample	Compressive Strength (MPa)	Average	Standard Deviation
1	1	18.14	19.18	1.08
	2	20.29		
	3	19.1		
3	1	34.14	33.75	0.52
	2	33.16		
	3	33.96		
5	1	36.58	36.64	0.59
	2	36.09		
	3	37.26		
7	1	39.02	38.43	0.64
	2	37.75		
	3	38.52		

Table A.2: Compressive strength data of grout cured at 1°C

Age (Days)	Sample	Compressive Strength (MPa)	Average	Standard Deviation
1	1	22.24	21.56	0.64
	2	21.46		
	3	20.97		
3	1	29.26	30.42	1.02
	2	31.16		
	3	30.84		
5	1	34.53	34.89	0.31
	2	35.02		
	3	35.11		
7	1	35.21	35.99	0.74
	2	36.68		
	3	36.09		

Table A.3: Compressive strength data of grout cured at -10°C

Age (Days)	Sample	Compressive Strength (MPa)	Average	Standard Deviation
1	1	20.97	20.55	1.18
	2	19.22		
	3	21.46		
3	1	27.99	26.72	1.13
	2	25.84		
	3	26.34		
5	1	33.55	32.32	1.18
	2	31.21		
	3	32.19		
7	1	31.7	32.51	0.74
	2	33.16		
	3	32.68		

Table A.4: Compressive strength data of grout cured at -10°C (12 hours initial curing)

Age (Days)	Sample	Compressive Strength (MPa)	Average	Standard Deviation
1/2 (12 Hours)	1	4.73	4.88	0.13
	2	4.92		
	3	4.99		
3	1	9.62	9.85	0.27
	2	10.14		
	3	9.79		
5	1	10.77	11.02	0.23
	2	11.22		
	3	11.07		
7	1	11.68	11.41	0.31
	2	11.07		
	3	11.49		

Table A.5: Compressive strength data of grout cured at -10°C (8 hours initial curing)

Age (Days)	Sample	Compressive Strength (MPa)	Average	Standard Deviation
1/3 (8 Hours)	1	0	0.00	0.00
	2	0		
	3	0		
3	1	2.07	1.95	0.11
	2	1.87		
	3	1.91		
5	1	2.97	3.27	0.28
	2	3.51		
	3	3.34		
7	1	3.81	3.54	0.29
	2	3.23		
	3	3.57		

Table A.6: Compressive strength data of grout cured at -20°C

Age (Days)	Sample	Compressive Strength (MPa)	Average	Standard Deviation
1	1	21.46	21.99	0.49
	2	22.43		
	3	22.08		
3	1	30.24	30.19	0.22
	2	29.95		
	3	30.38		
5	1	31.9	32.29	0.39
	2	32.68		
	3	32.29		
7	1	31.99	32.34	0.35
	2	32.68		
	3	32.34		

Table A.7: Tensile strength data of grout cured at ambient ($23 \pm 1^\circ\text{C}$)

Age (Days)	Sample	Tensile Strength (MPa)	Average	Standard Deviation
1	1	2.95	3.02	0.16
	2	3.20		
	3	2.90		
3	1	3.57	3.29	0.24
	2	3.18		
	3	3.12		
7	1	4.56	4.49	0.07
	2	4.48		
	3	4.42		
28	1	6.41	6.25	0.15
	2	6.12		
	3	6.23		

Table A.8: Tensile strength data of grout cured at -10°C

Age (Days)	Sample	Tensile Strength (MPa)	Average	Standard Deviation
1	1	2.89	3.01	0.12
	2	3.12		
	3	3.03		
3	1	3.39	3.18	0.22
	2	2.95		
	3	3.20		
7	1	3.06	3.22	0.18
	2	3.41		
	3	3.18		
28	1	3.55	3.68	0.37
	2	4.10		
	3	3.39		

Table A.9: Young's Modulus data of grout cured at ambient ($23 \pm 1^\circ\text{C}$)

Age	Load (lbs)	Stress (MPa)	Lateral Reading (mm)	Lateral Strain	Vertical Reading (mm)	Vertical Strain	Young's Modulus, E (MPa)	Poisson's Ratio, γ
7 Day	5000	2.74	0.003	1.47638E-05	0.029	0.0001087	20712	0.2285
	10000	5.49	0.008	3.93701E-05	0.066	0.0002474		
	15000	8.23	0.013	6.39764E-05	0.097	0.0003636		
	20000	10.97	0.02	9.84252E-05	0.132	0.0004948		
	25000	13.72	0.027	0.000132874	0.168	0.0006297		
	5000	2.74	0.004	1.9685E-05	0.041	0.0001537		
	10000	5.49	0.009	4.42913E-05	0.076	0.0002849		
	15000	8.23	0.015	7.38189E-05	0.113	0.0004235		
	20000	10.97	0.022	0.000108268	0.149	0.0005585		
	25000	13.72	0.029	0.000142717	0.186	0.0006972		
28 Day	5000	2.74	0.005	2.46063E-05	0.027	0.0001012	22712.5	0.2346
	10000	5.49	0.01	4.92126E-05	0.055	0.0002061		
	15000	8.23	0.015	7.38189E-05	0.085	0.0003186		
	20000	10.97	0.022	0.000108268	0.117	0.0004385		
	25000	13.72	0.028	0.000137795	0.149	0.0005585		
	5000	2.74	0.004	1.9685E-05	0.032	0.0001199		
	10000	5.49	0.01	4.92126E-05	0.067	0.0002511		
	15000	8.23	0.016	7.87402E-05	0.101	0.0003786		
	20000	10.97	0.021	0.000103346	0.135	0.0005060		
	25000	13.72	0.027	0.000132874	0.168	0.0006297		

Table A.10: Young's Modulus data of grout cured at -10°C

Age	Load (lbs)	Stress (MPa)	Lateral Reading (mm)	Lateral Strain	Vertical Reading (mm)	Vertical Strain	Young's Modulus, E (MPa)	Poisson's Ratio, γ
7 Day	5000	2.74	0.004	1.9685E-05	0.037	0.0001387	19971.2	0.23145
	10000	5.49	0.01	4.92126E-05	0.073	0.0002736		
	15000	8.23	0.016	7.87402E-05	0.11	0.0004123		
	20000	10.97	0.023	0.000113189	0.15	0.0005622		
	5000	2.74	0.008	3.93701E-05	0.035	0.0001312		
	10000	5.49	0.015	7.38189E-05	0.072	0.0002699		
	15000	8.23	0.021	0.000103346	0.105	0.0003936		
	20000	10.97	0.028	0.000137795	0.143	0.0005360		
28 Day	5000	2.74	0.006	2.95276E-05	0.033	0.0001237	20563	0.2322
	10000	5.49	0.012	5.90551E-05	0.068	0.0002549		
	15000	8.23	0.018	8.85827E-05	0.102	0.0003823		
	20000	10.97	0.024	0.00011811	0.138	0.0005172		
	5000	2.74	0.007	3.44488E-05	0.035	0.0001312		
	10000	5.49	0.014	6.88976E-05	0.07	0.0002624		
	15000	8.23	0.02	9.84252E-05	0.106	0.0003973		
	20000	10.97	0.027	0.000132874	0.144	0.0005397		

Table A.11: MIP data for grout cured for 1 day at ambient (23°C)

Pore Diameter (μm)	Incremental Pore Volume (mL/g)	Cumulative Intrusion (mL/g)
107.8672	0	0
71.3185	0.0005	0.0005
53.727	0.0009	0.0014
38.99	0.001	0.0024
35.7431	0.0006	0.003
28.5721	0.0024	0.0054
25.2089	0.0007	0.0061
22.5513	0.0013	0.0074
20.3938	0.0016	0.009
16.4683	0.0038	0.0128
13.3582	0.0026	0.0154
10.6897	0.0026	0.018
8.5479	0.0038	0.0218
8.033	0.0002	0.022
5.1879	0.0009	0.0229
4.5679	0.0003	0.0232
3.8121	0.0011	0.0243
2.9695	0.0018	0.0261
2.4356	0.0014	0.0275
1.9115	0.0014	0.0289
1.5587	0.0009	0.0298
1.2382	0.0008	0.0306
0.9796	0.001	0.0316
0.7971	0.0008	0.0324
0.6534	0.0008	0.0332
0.5118	0.001	0.0342
0.4119	0.0008	0.035
0.3347	0.0007	0.0357
0.2675	0.0007	0.0364
0.216	0.0008	0.0372
0.178	0.001	0.0382
0.1425	0.0013	0.0395
0.1125	0.0017	0.0412
0.0909	0.0025	0.0437
0.0737	0.005	0.0487
0.0594	0.0084	0.0571
0.0478	0.01	0.0671
0.0476	0.0001	0.0672
0.0382	0.0091	0.0763

0.031	0.0084	0.0847
0.0249	0.0075	0.0922
0.0202	0.0052	0.0974
0.0162	0.0042	0.1016
0.0144	0.0019	0.1035
0.013	0.0014	0.1049
0.0107	0.0021	0.107
0.0085	0.0018	0.1088
0.0071	0.0004	0.1092
0.0061	0.0008	0.11
0.0053	0.0005	0.1105
0.0047	0.0004	0.1109
0.0043	0.0004	0.1113
0.0039	0.0006	0.1119
0.0036	0.001	0.1129
0.0046	0.0011	0.114
0.006	0.0008	0.1148
0.0078	0.0005	0.1153
0.0102	0.0003	0.1156
0.0133	0.0002	0.1158
0.0172	0	0.1158
0.0222	-0.0003	0.1155
0.0292	-0.0006	0.1149
0.0373	-0.0009	0.114
0.0495	-0.0018	0.1122
0.0646	-0.0025	0.1097
0.0819	-0.0031	0.1066
0.1065	-0.0044	0.1022
0.142	-0.0059	0.0963
0.1776	-0.0048	0.0915
0.2366	-0.0057	0.0858
0.304	-0.0038	0.082
0.4256	-0.0033	0.0787
0.5306	-0.0013	0.0774
0.7067	-0.0011	0.0763
0.8857	-0.0006	0.0757
1.1066	-0.0006	0.0751
1.4695	-0.0006	0.0745
1.908	-0.0005	0.074
2.4232	-0.0005	0.0735
3.1829	-0.0005	0.073
4.0175	-0.0005	0.0725
6.6126	-0.0009	0.0716

Table A.12: MIP data for grout cured for 7 days at ambient (23°C)

Pore Diameter (μm)	Incremental Intrusion (mL/g)	Cumulative Intrusion (mL/g)
107.4817	0	0
71.3757	0.0003	0.0003
53.6886	0.0001	0.0004
38.971	0.0002	0.0006
35.718	0.0001	0.0007
28.5655	0.0003	0.001
25.1992	0.0001	0.0011
22.5461	0.0002	0.0013
20.397	0.0001	0.0014
16.465	0.0001	0.0015
13.3595	0.0003	0.0018
10.689	0.0004	0.0022
8.2248	0	0.0022
5.0469	0.0002	0.0024
4.5629	0	0.0024
3.7947	0.0004	0.0028
2.9529	0.0007	0.0035
2.4316	0.0013	0.0048
1.8934	0.0014	0.0062
1.5506	0.0013	0.0075
1.2327	0.0028	0.0103
0.9899	0.0029	0.0132
0.7956	0.0039	0.0171
0.6518	0.005	0.0221
0.5107	0.0048	0.0269
0.4126	0.0033	0.0302
0.335	0.0037	0.0339
0.2676	0.0032	0.0371
0.2159	0.002	0.0391
0.1777	0.0018	0.0409
0.1425	0.0025	0.0434
0.1125	0.0053	0.0487
0.0909	0.007	0.0557
0.0737	0.006	0.0617
0.0594	0.0053	0.067
0.0476	0.005	0.072
0.0382	0.0041	0.0761
0.031	0.0038	0.0799
0.0249	0.0037	0.0836

0.0202	0.0026	0.0862
0.0162	0.002	0.0882
0.0144	0.0007	0.0889
0.013	0.0005	0.0894
0.0107	0.001	0.0904
0.0085	0.0011	0.0915
0.0071	0.0011	0.0926
0.0061	0.001	0.0936
0.0053	0.0016	0.0952
0.0047	0.0012	0.0964
0.0043	0.0019	0.0983
0.0039	0.0016	0.0999
0.0036	0.0008	0.1007
0.0046	0.0018	0.1025
0.006	0.0007	0.1032
0.0078	0.0004	0.1036
0.0102	0.0002	0.1038
0.0133	0	0.1038
0.0172	-0.0002	0.1036
0.0222	-0.0004	0.1032
0.0292	-0.0006	0.1026
0.0373	-0.0007	0.1019
0.0495	-0.001	0.1009
0.0646	-0.0013	0.0996
0.082	-0.0016	0.098
0.1066	-0.0024	0.0956
0.1421	-0.0034	0.0922
0.1775	-0.0032	0.089
0.2367	-0.0042	0.0848
0.3041	-0.0035	0.0813
0.425	-0.0039	0.0774
0.5307	-0.0021	0.0753
0.7049	-0.0021	0.0732
0.8803	-0.0013	0.0719
1.1097	-0.0012	0.0707
1.4412	-0.0012	0.0695
1.9168	-0.001	0.0685
2.4626	-0.0006	0.0679
3.1403	-0.0005	0.0674
4.0598	-0.0004	0.067
6.3971	-0.0005	0.0665

Table A.13: MIP data for grout cured for 3 days at -10°C

Pore Diameter (μm)	Incremental Pore Volume (mL/g)	Cumulative Intrusion (mL/g)
107.6613	0	0
71.2716	0.0003	0.0003
53.6674	0.0002	0.0005
38.9513	0.0006	0.0011
35.711	0.0001	0.0012
28.5585	0.0002	0.0014
25.1923	0.0001	0.0015
22.5451	0.0003	0.0018
20.3963	0.0004	0.0022
16.4676	0.0006	0.0028
13.3528	0.0004	0.0032
10.6853	0.0023	0.0055
8.5446	0.0012	0.0067
8.124	0.0001	0.0068
5.016	0.0004	0.0072
4.6132	0.0001	0.0073
3.7609	0.0005	0.0078
2.9664	0.0015	0.0093
2.4542	0.0013	0.0106
1.9058	0.0013	0.0119
1.5538	0.0013	0.0132
1.2316	0.0015	0.0147
0.9816	0.0015	0.0162
0.7996	0.001	0.0172
0.6512	0.0011	0.0183
0.5116	0.0017	0.02
0.4122	0.002	0.022
0.3351	0.002	0.024
0.2672	0.0017	0.0257
0.2158	0.0012	0.0269
0.1782	0.0011	0.028
0.1424	0.0014	0.0294
0.1125	0.0017	0.0311
0.091	0.0019	0.033
0.0737	0.0037	0.0367
0.0594	0.0078	0.0445
0.0475	0.0094	0.0539
0.0382	0.0071	0.061
0.031	0.0076	0.0686
0.0249	0.0061	0.0747

0.0202	0.0046	0.0793
0.0162	0.0041	0.0834
0.0144	0.0019	0.0853
0.013	0.0016	0.0869
0.0107	0.0027	0.0896
0.0085	0.0025	0.0921
0.0071	0.0015	0.0936
0.0061	0.0012	0.0948
0.0053	0.0013	0.0961
0.0047	0.0005	0.0966
0.0043	0.0012	0.0978
0.0039	0.0012	0.099
0.0036	0.001	0.1
0.0046	0.0011	0.1011
0.006	0.0008	0.1019
0.0078	0.0003	0.1022
0.0102	0.0002	0.1024
0.0133	0	0.1024
0.0172	-0.0004	0.102
0.0222	-0.0008	0.1012
0.0292	-0.0014	0.0998
0.0373	-0.0017	0.0981
0.0495	-0.0027	0.0954
0.0646	-0.0032	0.0922
0.082	-0.0033	0.0889
0.1066	-0.0042	0.0847
0.1421	-0.005	0.0797
0.1778	-0.0039	0.0758
0.2367	-0.0046	0.0712
0.3045	-0.0034	0.0678
0.4254	-0.0032	0.0646
0.53	-0.0015	0.0631
0.7052	-0.0014	0.0617
0.8789	-0.0009	0.0608
1.1063	-0.0008	0.06
1.4388	-0.0009	0.0591
1.8743	-0.0008	0.0583
2.4182	-0.0006	0.0577
3.1602	-0.0006	0.0571
3.9805	-0.0005	0.0566
6.5197	-0.0008	0.0558

Table A.14: MIP data for grout cured for 7 days at -10°C

Pore Diameter (μm)	Incremental Pore Volume (mL/g)	Cumulative Intrusion (mL/g)
107.8672	0	0
71.3185	0.0003	0.0003
53.727	0.0002	0.0005
38.99	0.0003	0.0008
35.7431	0	0.0008
28.5721	0.0002	0.001
25.2089	0.0001	0.0011
22.5513	0.0001	0.0012
20.3938	0.0001	0.0013
16.4683	0.0006	0.0019
13.3582	0.0009	0.0028
10.6897	0.0012	0.004
8.5479	0.0031	0.0071
7.9605	0.0001	0.0072
5.1595	0.0016	0.0088
4.5484	0.0016	0.0104
3.7995	0.0017	0.0121
2.9623	0.0023	0.0144
2.431	0.0016	0.016
1.9089	0.002	0.018
1.5571	0.0013	0.0193
1.2373	0.001	0.0203
0.979	0.0012	0.0215
0.7967	0.0008	0.0223
0.6531	0.001	0.0233
0.5116	0.0017	0.025
0.4118	0.0012	0.0262
0.3346	0.0014	0.0276
0.2674	0.0013	0.0289
0.2159	0.0012	0.0301
0.178	0.0012	0.0313
0.1425	0.0015	0.0328
0.1125	0.0015	0.0343
0.0909	0.0017	0.036
0.0737	0.003	0.039
0.0594	0.0071	0.0461
0.0478	0.0092	0.0553
0.0476	0.0001	0.0554
0.0382	0.0084	0.0638
0.031	0.0078	0.0716

0.0249	0.0068	0.0784
0.0202	0.0052	0.0836
0.0162	0.0044	0.088
0.0144	0.002	0.09
0.013	0.0016	0.0916
0.0107	0.0026	0.0942
0.0085	0.0023	0.0965
0.0071	0.0014	0.0979
0.0061	0.0011	0.099
0.0053	0.001	0.1
0.0047	0.001	0.101
0.0043	0.0012	0.1022
0.0039	0.0013	0.1035
0.0036	0.0016	0.1051
0.0046	0.0012	0.1063
0.006	0.0004	0.1067
0.0078	0.0002	0.1069
0.0102	0	0.1069
0.0133	-0.0002	0.1067
0.0172	-0.0005	0.1062
0.0222	-0.0007	0.1055
0.0292	-0.0011	0.1044
0.0373	-0.0015	0.1029
0.0495	-0.0024	0.1005
0.0646	-0.003	0.0975
0.0819	-0.0034	0.0941
0.1065	-0.0046	0.0895
0.142	-0.0058	0.0837
0.1776	-0.0046	0.0791
0.2366	-0.0049	0.0742
0.304	-0.0032	0.071
0.4256	-0.0027	0.0683
0.5305	-0.0011	0.0672
0.7066	-0.001	0.0662
0.8856	-0.0007	0.0655
1.1064	-0.0006	0.0649
1.469	-0.0007	0.0642
1.9072	-0.0006	0.0636
2.4219	-0.0005	0.0631
3.1804	-0.0006	0.0625
4.0134	-0.0005	0.062
6.6016	-0.0008	0.0612

CURRICULUM VITAE

Identification Douglas J. Provost-Smith, b. London ON, 1991

Post-secondary Education

2014 – 2016 Master of Engineering Science, MEngSc
The University of Western Ontario, London, Ontario, Canada

2010 – 2014 Bachelor of Engineering Science, BEngSc
The University of Western Ontario, London, Ontario, Canada

Honours and Awards

2014 Dean's Honour List, The University of Western Ontario

2013 Dean's Honour List, The University of Western Ontario

2013 125th Anniversary Alumni Award in Engineering

Related Work Experience

2014-2016 Research Assistant, Teaching Assistant
The University of Western Ontario, London, Ontario, Canada

Publications:

Provost, D. J., Elsayed, M., & Nehdi, M. L., "Investigation of Grouted Dowel Connections for Precast Wall Construction." Submitted to *ACI Structural Journal*.

Provost, D. J., Elsayed, M., & Nehdi, M. L., "Early-age Exposure of Grouted Precast Wall Connections to Subfreezing Curing Temperatures." Submitted to *Construction and Building Materials*.

Provost, D. J., Elsayed, M., & Nehdi, M. L., (2016) "Investigation of Grouted Precast Concrete Wall Connections at Subfreezing Conditions." *Proceedings of the CSCE 5th International Materials Specialty Conference*, London, ON. MAT-719.

Elsayed, M., Provost, D. J., and Nehdi, M. L. (2016) "Bond Behaviour of Grouted Connections Under Monotonic Tensile Loads." *Proceedings of the CSCE 5th International Materials Specialty Conference*, London, ON. MAT-723.